NIST Technical Note 1390

Noise Temperature Measurements on Wafer

J. Randa

Electromagnetic Fields Division
Electronics and Electrical Engineering Laboratory
National Institute of Standards and Technology
325 Broadway
Boulder, Colorado 80303-3328

March 1997

U.S. DEPARTMENT OF COMMERCE, William M. Daley, Secretary
TECHNOLOGY ADMINISTRATION, Mary L. Good, Under Secretary for Technology
NATIONAL INSTITUTE OF STANDARDS AND TECHNOLOGY, Arati Prabhakar, Director

CONTENTS

NOISE TEMPERATURE MEASUREMENTS ON WAFER

J. Randa
Electromagnetic Fields Division
National Institute of Standards and Technology
Boulder, CO 80303

The NIST Noise Project has developed the theoretical formalism and experimental methods for performing accurate noise-temperature measurements on wafer. This report presents the theoretical formulation and describes the design, methods, and results of tests performed to verify our ability to measure on-wafer noise temperature. With known off-wafer noise sources, several different configurations were used to obtain different, known, on-wafer noise temperatures. These were then measured, and the results were compared to predictions. Good agreement was found, with a worst-case disagreement of 2.6 percent. An uncertainty analysis of the measurements resulted in an estimated standard uncertainty (1σ) of 1.1 percent or less for most values of noise temperature. The tests also confirm our ability to produce known noise temperatures on wafer.

Keywords: noise; noise measurement; noise temperature; on-wafer noise; thermal noise

1. INTRODUCTION

The move toward miniaturization and on-wafer integration in the electronics industry has brought with it the need for accurate, reproducible measurements of microwave properties of devices and structures on wafer. An area of considerable importance and interest is the measurement of noise parameters on wafer, in particular the noise figure of a two-port device, such as some variety of low-noise transistor. The noise figure of a device is a measure of the noise added to the input signal by the device itself. It is determined by measuring the output noise power from the device for different known levels of input noise power. Because the noise figure of a device depends on the impedance of the input source, it must be measured for several different input impedances to characterize that dependence. Alternatively, if there is a single input impedance of interest, for example, 50 Ω, then the noise figure can be measured at just that one impedance. A good deal of work has been done over the past several years to develop and improve techniques for measurement of noise figure on wafer [1-11]. Methods and even commercial systems exist for such measurements. There is always room for improvement and extension of such methods, of course, but a more pressing need at present appears to be in the areas of accuracy assessment, traceability, and general quality assurance.

To address this need, the Noise Metrology Project, in the Microwave Metrology Group of the National Institute of Standards and Technology (NIST), is developing the capability to measure noise figure (NF) on wafer. This work builds on our long-established ability in noise-temperature measurements in waveguide and coaxial structures [12,13] as well as on recent work [14] on coaxial noise-figure measurements. The first major step in the development of an on-wafer noise-figure capability is to establish our ability to measure noise temperature on wafer and to determine the accuracy of those measurements. This is a necessary first step because the measurement of the noise figure consists of a series of measurements of noise power (or equivalently noise *temperature*) at the output of the device under test (DUT) for different known input noise sources. Thus, in order to measure noise figure on wafer, it is necessary to be able both to produce known on-wafer noise temperatures and to measure unknown noise temperatures (or their ratios).

Besides its necessity for noise-figure measurements, a NIST capability in on-wafer noise-temperature measurement would be useful in its own right. It could serve as the basis for a measurement service for on-wafer noise-temperature transfer standards, or for intercomparisons involving such transfer standards. Such a service or series of comparisons would enable private industry to verify their own on-wafer noise measurements. For these reasons, we have developed the necessary analytical foundation and performed a series of measurements to test our ability to measure noise temperature on wafer. In doing so, we have also verified our ability to produce known noise temperatures on wafer.

On-wafer noise measurements present a number of difficulties or challenges not encountered in traditional noise measurements with waveguide or coaxial connections. One problem is that it is difficult to obtain a good impedance match between the measurement system, the probe, and the on-wafer system. Consequently, the assumption of a well-matched system is not justified, and scalar quantities, such as the noise figure for a 50 Ω system, cannot be measured directly. Furthermore, even when corrections are made for the relevant mismatch factors, the uncertainties in those corrections are substantial, and they can lead to a significant increase in the uncertainty in the noise temperature or noise figure. Several other problems can be associated specifically with either the wafer environment or the probe. On-wafer transmission lines typically have significant losses, due mostly to dielectric losses in the substrate but also to resistive losses in the thin conductor strips. The presence of these losses changes the form of the various power equations (and consequently of the mismatch factors, available-power ratios, etc.) used in computing the noise temperature of a device under test from the measured powers. Therefore, the entire formulation of the radiometer equation must be reexamined and rederived. Another potential problem associated with the wafer is that it is an open environment, which raises the possibility of outside radiation entering the system and contaminating the measurements. For its part, the probe, which serves as a transition from the transmission line on wafer to the coaxial line of the measurement instrumentation, is unlike ordinary transitions in at least two important respects. It has significant loss (of order 0.5 dB to 1.5 dB), and there are no standard noise sources which can be connected directly to the

wafer side of the probe. These two facts preclude the use of the methods which NIST normally employs to evaluate and correct for the effects of adapters and transitions. Thus we cannot treat the probe as just another adapter. We must characterize it by direct measurement of its S-parameters, and that characterization will prove to be the principal source of uncertainty in our measurements. These difficulties all occur before we even begin the measurements. They will be considered in some detail below, as will several additional theoretical concerns and practical problems which arise during the course of the measurements.

The remainder of this paper is organized as follows. The next section presents the theoretical background and foundations for on-wafer noise-temperature measurements. It establishes notation, reviews the expression for power, gives the connection between travelling-wave amplitudes and noise temperature in the case of lossy transmission lines, derives the relevant radiometer equation and the expressions for mismatch factor and available power ratio for lossy lines, and discusses the use of the "pseudo-waves" of Marks and Williams [15]. Section 3 is devoted to the measurements. It describes the experimental setup, presents the different configurations of noise sources which were measured, provides an uncertainty analysis, and reports the measurement results. Section 4 contains a discussion and summary of the results and of some of the techniques used. There are two appendices, which are devoted to algebraic details.

2. THEORETICAL BACKGROUND

2.1 Normalization and Power

In this section we establish notation and normalization conventions. Considerable detail is presented, in part for future reference, but also because there are some necessary departures from the "usual" [16, 17] treatments. Losses in transmission lines on wafer can be significant, resulting in modifications of some old familiar results, which rely on lossless or low-loss lines. Since the lossy case is still viewed as a bit of a curiosity (not to say aberration) by some, it may be useful to be specific about some of the basics and the form they take with our choice of notation.

Much of the development in this section parallels that of reference [15], but we use a somewhat different notation, which we find more convenient for this application.

For a single mode a of a uniform waveguide, the electromagnetic fields of travelling waves propagating in the positive or negative z direction take the form

$$\begin{aligned} \vec{E}_a^{\pm}(\vec{x}_t, z) &= c_a^{\pm} e^{\mp\gamma_a z}(\vec{e}_{at} \pm \vec{e}_{az}), \\ \vec{H}_a^{\pm}(\vec{x}_t, z) &= \pm c_a^{\pm} e^{\mp\gamma_a z}(\vec{h}_{at} \pm \vec{h}_{az}), \end{aligned} \tag{1}$$

with an implicit time dependence $e^{j\omega t}$. In eq (1), $c_a^{\pm}$ is the amplitude of the wave in the $\pm z$ direction, $\vec{e}_{at}$ and $\vec{h}_{at}$ are in the transverse plane, $\vec{e}_{az}$ and $\vec{h}_{az}$ are longitudinal, and all four depend only on the transverse coordinates, $\vec{e}_{at} = \vec{e}_{at}(\vec{x}_t)$, $\vec{e}_{az} = e_{az}(\vec{x}_t)\,\hat{z}$, etc. For $\vec{E}_a^{\pm}$ and $\vec{H}_a^{\pm}$ to satisfy Maxwell's equations, the modal functions must satisfy

$$\begin{aligned} \gamma_a \vec{h}_{at} + \vec{\nabla} h_{az} &= j\omega\epsilon\,\hat{z}\times\vec{e}_{at}, \\ \vec{h}_{az} &= \frac{j}{\omega\mu}\vec{\nabla}\times\vec{e}_{at}, \\ \vec{e}_{az} &= -\frac{j}{\omega\epsilon}\vec{\nabla}\times\vec{h}_{at}. \end{aligned} \tag{2}$$

Note that eq (2) could be used to write all other components in terms of just $\vec{e}_{at}$. Consequently, in the normalization considerations, we need (can) only fix the normalization of $\vec{e}_{at}$, and the normalization of the other three functions is then fixed by Maxwell's equations. When travelling waves in both directions are present, the fields from mode a can be written as

$$\begin{aligned} \vec{E}_a &= (a_a + b_a)\,\vec{e}_{at} + (a_a - b_a)\,\vec{e}_{az}, \\ \vec{H}_a &= (a_a - b_a)\,\vec{h}_{at} + (a_a + b_a)\,\vec{h}_{az}, \end{aligned} \tag{3}$$

where we have introduced

$$a_a = a_a(z) \equiv c_a^+ e^{-\gamma_a z} ,$$
$$b_a = b_a(z) \equiv c_a^- e^{\gamma_a z} . \tag{4}$$

The (complex) power flowing in the positive z direction can be written as

$$\mathcal{P} = \int \vec{E}_a \times \vec{H}_a^* \cdot \hat{z}\, d^2x_t = \left[|a_a|^2 - |b_a|^2 - 2j\, Im(a_a b_a^*) \right] I_a , \tag{5}$$

with

$$\begin{aligned} I_a &\equiv \int \vec{e}_{at} \times \vec{h}_{at}^* \cdot \hat{z}\, d^2x_t \\ &= \int \vec{e}_{at} \times \left\{ \frac{1}{\gamma_a} \left[j\omega\epsilon\, \hat{z} \times \vec{e}_{at} - \nabla \left(\frac{j}{\omega\mu} \nabla \times \vec{e}_{at} \cdot \hat{z} \right) \right] \right\}^* \cdot \hat{z}\, d^2x_t . \end{aligned} \tag{6}$$

The physical power is then given by

$$\begin{aligned} P_a &= Re(\mathcal{P}) = \left[|a_a|^2 - |b_a|^2 + 2\tan\zeta_a\, Im(a_a b_a^*) \right] Re(I_a) , \\ \tan\zeta_a &\equiv \frac{Im(I_a)}{Re(I_a)} , \end{aligned} \tag{7}$$

where ζ_a has been defined as the phase of the integral I_a. This expression for the power differs from the familiar (lossless) form by the presence of the cross term proportional to $\tan\zeta_a$, which is determined by Maxwell's equations via eq (6). In the lossless case, γ_a is purely imaginary, I_a is real, and $\tan\zeta_a$ vanishes. In general, however, the cross term is present [15,18], and it necessitates modifications of the usual expressions for quantities involving power or power ratios (mismatch factors, efficiencies, etc.).

We now turn to the question of normalization. Basically, there are two choices to be made. One is whether we are more interested in the fields or in power and S-parameter calculations. The second (rather trivial) consideration is where we want to put the dimensions — in a_a and b_a or in $\vec{e}_a$ and $\vec{h}_a$. In the present work we are interested in power and S-parameter calculations, and we shall use a "power normalization." This consists in setting

$$Re(I_a) = Re\left\{\int \vec{e}_{at}\times\left\{\frac{1}{\gamma_a}\left[j\omega\epsilon\hat{z}\times\vec{e}_{at} - \vec{\nabla}\left(\frac{j}{\omega\mu}\vec{\nabla}\times\vec{e}_{at}\cdot\hat{z}\right)\right]\right\}^{*}\cdot\hat{z}\, d^2x_t\right\} = 1. \quad (8)$$

Note that this is a condition on $\vec{e}_{at}$ only; the normalizations of the other components are determined from eq (2). The expression for the power in mode a then becomes

$$P_a = \left[|a_a|^2 - |b_a|^2 + 2\tan\zeta_a Im(a_a b_a^*)\right]. \quad (9)$$

The dimensions of the various quantities in this scheme are

$$a_a\,[\sqrt{W}]\ ,\ b_a\,[\sqrt{W}]\ ,\ c_a^{\pm}\,[\sqrt{W}]\ ,\ \vec{e}_a\,[\sqrt{\Omega/m}]\ ,\ \vec{h}_a\left[\frac{1}{\sqrt{\Omega}\,m}\right]. \quad (10)$$

As mentioned above, we could choose to shift units around so that, for example, a_a, b_a, and $c_a^{\pm}$ were all dimensionless and $\vec{e}_a$ had dimensions V/m, but for present purposes we shall use eqs (9) and (10). The remaining practical question is what is the physical significance or interpretation of ζ_a, and how does one determine or measure it? Comparison to reference [15] indicates that the integral which we are calling I_a is their p_0. The phase of I_a is then the same as the phase of p_0 and therefore of (their) Z_0. Thus ζ_a is just the phase of the characteristic impedance of the line (for that mode). Measurement of ζ_a will be discussed below. For those not familiar with reference [15], the connection between I_a and the impedance is clearer in the alternative normalization scheme discussed in the next paragraph.

An alternative normalization scheme (which will *not* be used in this paper) is what could be called field normalization. If our interest were primarily in the fields, it would be most natural to choose a normalization like $\int|\vec{e}_{at}|^2\, d^2x_t = 1$. With this normalization choice, the dimensions are $\vec{e}\,[m^{-1}]$, $\vec{h}\,[(\Omega\cdot m)^{-1}]$, and a_a[V], b_a[V], $c_a^{\pm}$[V]. The integral I_a then has dimension Ω^{-1}, and so it is natural to identify it with an (inverse) impedance characterizing the mode a. In general, there is no single wave impedance for

a general mode (cf. reference [19]), but for the simple case of $\vec{h}_{at} \cdot \vec{e}_{at} = 0$, we have $\vec{h}_{at} \times \hat{z} = Z_a^{-1} \vec{e}_{at}$, and therefore $I_a = (1/Z_a^*) \int |\vec{e}_{at}|^2 \, d^2x_t = 1/Z_a^*$. Thus the phase of I_a is the same as the phase of Z_a. In this normalization, the expression for power involves $Re(1/Z_a^*)$, which is somewhat cumbersome to carry through power calculations.

2.2 Generator Waves and Noise Temperature for Lossy Lines

To relate travelling-wave amplitudes to noise temperature, we need an expression for the available power which is valid for a lossy line. Consider the general configuration of figure 1. In terms of the amplitude of the generator wave ($\hat{b}_G$) and the reflection coefficient $\Gamma_a \equiv b_a/a_a$, eq (9) for the delivered power can be written as

$$\begin{aligned} P_a^{del} &= |a_a|^2 \left[1 - |\Gamma_a|^2 - 2 \tan\zeta_a \, Im\Gamma_a\right] \\ &= \frac{|\hat{b}_G|^2}{|1 - \Gamma_a \Gamma_G|^2} \left[1 - |\Gamma_a|^2 - 2 \tan\zeta_a \, Im\Gamma_a\right] . \end{aligned} \tag{11}$$

The available power is obtained by replacing Γ_a by the expression for the optimal reflection coefficient, which is no longer simply the complex conjugate of the generator reflection coefficient, $\Gamma^{opt} = \Gamma_G^*$, but rather

$$\Gamma_a^{opt} = \frac{\Gamma_G^* - j \tan\zeta_a}{1 - j \Gamma_G^* \tan\zeta_a} . \tag{12}$$

To calculate the available power, we set $\Gamma_a = \Gamma_a^{opt}$ in eq (11). A little algebra then yields

$$P^{avail} = \frac{|\hat{b}_G|^2}{\left[1 - |\Gamma_G|^2 - 2 \, Im\Gamma_G \tan\zeta\right] \cos^2\zeta} , \tag{13}$$

where we have suppressed the subscript *a* since we will be assuming a single mode in the present work. For a thermal noise source at noise temperature T, we can then equate the available power to $k_B TB$, thereby obtaining

$$\langle|\hat{b}_G|^2\rangle = k_B B T[1 - |\Gamma_G|^2 - 2\, Im\Gamma_G \tan\zeta]\cos^2\zeta\,, \qquad (14)$$

where the brackets < > refer to the time average.

Similar expressions can be derived for the intrinsic noise sources in a passive, linear two-port, figure 2. The two-port can be characterized by

$$\begin{pmatrix} b_1 \\ b_2 \end{pmatrix} = S \begin{pmatrix} a_1 \\ a_2 \end{pmatrix} + \begin{pmatrix} \hat{b}_1 \\ \hat{b}_2 \end{pmatrix}, \qquad (15)$$

where S is the usual 2x2 matrix of scattering parameters, and $\hat{b}_1$, $\hat{b}_2$ are the emerging wave amplitudes due to the internal thermal noise sources. To fix $\hat{b}_2$ we assume that the entire circuit is in thermal equilibrium at temperature T. (For those worried about quantum effects, what we really mean is at the physical temperature which corresponds to a noise temperature of T.) To obtain an expression for $\langle|\hat{b}_2|^2\rangle$, we choose $\Gamma_G = 0$ in figure 2 and require that the available power at plane 2 be given by $k_B TB$. This leads to eq (14), but with the reflection coefficient and generator wave amplitude being those appropriate to plane 2, that is those of the generator-two-port system. If we refer to the generator plus the two-port as GS, then

$$\langle|\hat{b}_{GS}|^2\rangle = k_B B T[1 - |\Gamma_{GS}|^2 - 2\, Im\Gamma_{GS} \tan\zeta_2]\cos^2\zeta_2\,, \qquad (16)$$

where ζ_2 is the phase of the characteristic impedance at plane 2, and where

$$\hat{b}_{GS} = b_2(a_2=0) = \hat{b}_2 + S_{21}\frac{\hat{b}_G + \Gamma_G \hat{b}_1}{1 - \Gamma_G S_{11}}\,,$$

$$\Gamma_{GS} = S_{22} + \frac{S_{12}S_{21}\Gamma_G}{1 - \Gamma_G S_{11}}\,. \qquad (17)$$

We then set $\Gamma_G = 0$ in eq (17), substitute it into eq (16), use eq (14) for $\langle|\hat{b}_G|^2\rangle$, and solve for $\langle|\hat{b}_1|^2\rangle$. The result is

$$\langle|\hat{b}_2|^2\rangle = k_B TB[(1 - |S_{22}|^2 - 2\tan\zeta_2\, ImS_{22})\cos^2\zeta_2 - |S_{21}|^2\cos^2\zeta_1]\,, \qquad (18)$$

where ζ_1 is the phase of the characteristic impedance at plane 1. A similar

exercise can be applied at plane 1, lumping together the two-port and the load and considering the available power from them at plane 1. The result is

$$\langle|\hat{b}_1|^2\rangle = k_B T B\left[\left(1 - |S_{11}|^2 - 2\tan\zeta_1\, Im S_{11}\right)\cos^2\zeta_1 - |S_{12}|^2\cos^2\zeta_2\right]. \quad (19)$$

The expression for the correlation between the two amplitudes can be derived by using a nonzero Γ_G in figure 2. Again we require that the available power at plane 2 (and at plane 1 when G and L are interchanged) satisfy eq (14), using the appropriate Γ_G and $\hat{b}_G$ of course. After a bit of algebra, we obtain

$$\langle\hat{b}_1\,\hat{b}_2^*\rangle = -k_B T B\left[S_{21}^*\left(S_{11} + j\tan\zeta_1\right)\cos^2\zeta_1 + S_{12}\left(S_{22}^* - j\tan\zeta_2\right)\cos^2\zeta_2\right]. \quad (20)$$

It is reassuring to note that when ζ_1, $\zeta_2 = 0$, eqs (18), (19), and (20) reduce to Wait's results [20]. Note that this result does not assume any relationship between the various scattering parameters, such as S_{12} and S_{21}.

2.3 Mismatch, Available Power, Etc.

The expressions for delivered and available power, eqs (11) and (13), lead directly to equations for the mismatch factor and available power ratio which are valid for lossy transmission lines or waveguides. For the mismatch factor we use eq (11) for the delivered power and eq (13) for the available power, resulting in

$$M \equiv \frac{P^{del}}{P^{avail}} = \frac{\left[1 - |\Gamma_L|^2 - 2\tan\zeta\, Im\Gamma_L\right]\left[1 - |\Gamma_G|^2 - 2\tan\zeta\, Im\Gamma_G\right]\cos^2\zeta}{|1 - \Gamma_L\Gamma_G|^{2//}}. \quad (21)$$

For a passive two-port device, the available power ratio is defined as $\alpha_{21} = P_2^{avail}/P_1^{avail}$. Referring to figure 2, the available power at plane 1 is given by eq (13), with $\zeta = \zeta_1$. At plane 2, eq (13) again applies, with $\zeta = \zeta_2$, but $\hat{b}_G$ and Γ_G now refer to the combination of generator plus two-port. These are given in eq (17) for the more general case allowing for internal sources in the two-port. For evaluation of α_{21} we want to neglect any

internal sources. Thus we use eq (17) with $\hat{b}_1 = \hat{b}_2 = 0$, and the available powers take the form

$$P_1^{avail} = \frac{|\hat{b}_G|^2}{[1 - |\Gamma_G|^2 - 2\tan\zeta_1\, Im\Gamma_G]\cos^2\zeta_1},$$
$$P_2^{avail} = \frac{|S_{21}|^2\,|\hat{b}_G|^2}{|1 - \Gamma_G S_{11}|^2[1 - |\Gamma_{GS}|^2 - 2\,Im\Gamma_{GS}\tan\zeta_2]\cos^2\zeta_2}. \quad (22)$$

The available power ratio is then given by

$$\alpha_{21} = \frac{|S_{21}|^2\,[1 - |\Gamma_G|^2 - 2\,Im\Gamma_G\tan\zeta_1]\,\cos^2\zeta_1}{|1 - \Gamma_G S_{11}|^2\,[1 - |\Gamma_{GS}|^2 - 2\,Im\Gamma_{GS}\tan\zeta_2]\,\cos^2\zeta_2}, \quad (23)$$

with Γ_{GS} given by eq (17). We could substitute the explicit expression for Γ_{GS} into eq (23), but the result is not particularly enlightening. For the case of lossless lines, $\zeta_1 = \zeta_2 = 0$, α_{21} reduces to

$$\alpha_{21} = \frac{|S_{21}|^2\,[1 - |\Gamma_G|^2]}{|1 - \Gamma_G S_{11}|^2\,[1 - |\Gamma_{GS}|^2]}, \quad (24)$$

which is the familiar form for an attenuator.

A lossy two-port, such as an attenuator, is not a perfectly passive device: it contains noise sources. Consequently, the available power at plane 2 includes not just the contribution from the attenuated available power at plane 1, but also a contribution from the sources between planes 1 and 2. General considerations can be used to show that the available power at plane 2 is given by

$$P_2^{avail} = \alpha_{21}\,P_1^{avail} + [1 - \alpha_{21}]\,kBT_A, \quad (25)$$

where T_A is the noise temperature of the attenuator. Equation (25) can also be derived directly from travelling-wave amplitudes, S-parameters, reflection coefficients, and some algebra. This is done in Appendix A.

2.4 Radiometer Equation and Noise Temperature On Wafer

We can now obtain the explicit expression for the radiometer equation, relating the noise temperature on wafer to the noise temperatures of the standards and the powers delivered to the radiometer. The general configuration and relevant reference planes are shown in figure 3. The radiometer itself also contained an isolator, so that there were isolators immediately to the left and right of plane 0. Available powers will be denoted by capital P, and delivered powers by lowercase p. The subscript on an available power generally indicates the device, except in the case of P_a, where it indicates the ambient, $P_a = kBT_a$. The subscripts on the delivered powers and mismatch factors will indicate the reference plane and the configuration. Thus $p_{2,x}$ refers to the delivered power at plane 2 when the DUT (x) is connected. For an isolated radiometer, the derivation follows the basic treatment by Daywitt [13], with a few notational changes. The power delivered to the radiometer, at plane 0, when the switch is connected to the DUT at plane 7, is given by

$$p_{0,x} = M_{0,x}\alpha_{07}P_x + M_{0,x}[1-\alpha_{07}]P_a + p_{ex}, \tag{26}$$

where P_{ex} is the intrinsic effective input noise power of the radiometer for this configuration. Similarly,

$$\begin{aligned} p_{0,s} &= M_{0,s}\alpha_{03}P_s + M_{0,s}[1-\alpha_{03}]P_a + p_{es}, \\ p_{0,a} &= M_{0,a}P_a + p_{ea}. \end{aligned} \tag{27}$$

Due to the isolator to the left of plane 0, the intrinsic effective input noise power of the radiometer is (approximately) independent of the source configuration, $p_{ex} \approx p_{es} \approx p_{ea}$. Combining eqs (26) and (27), we obtain Daywitt's form [13],

$$T_x = T_a + (T_s - T_a)\frac{M_{0,s}\alpha_{03}}{M_{0,x}\alpha_{07}}\frac{Y_x - 1}{Y_s - 1} + (\Delta T_x)_{is}, \tag{28}$$

where $Y_x = p_x/p_a$, $Y_s = p_s/p_a$, and where $(\Delta T_x)_{is}$ is the error in T_x due to the (small) effect of an imperfect isolator. The general expression for the ratio of $M\alpha$'s is rather cumbersome. It simplifies somewhat if we use the identity

(in the notation of figure 2)

$$(1 - S_{22}\Gamma_L)\,(1 - \Gamma_G\Gamma_{1,L}) = (1 - S_{11}\Gamma_G)\,(1 - \Gamma_{2,G}\Gamma_L)\,, \tag{29}$$

and furthermore note that $\zeta_3 \approx 0$, since plane 3 is in a coaxial line with real impedance, and that $S_{22}(7\text{–}0) \approx S_{22}(3\text{–}0)$, due to the isolators. As a matter of notation, for reflection coefficients or mismatch factors with two subscripts, the first subscript refers to the reference plane, and the second indicates the direction of incidence. Thus $\Gamma_{1,L}$ is the reflection coefficient from the load at plane 1. The ratio of $M\alpha$'s can then be written as

$$\frac{M_{0,s}\alpha_{03}}{M_{0,x}\alpha_{07}} = \frac{|S_{21}(3\text{-}0)|^2}{|S_{21}(7\text{-}0)|^2}\,\frac{|1 - \Gamma_x\Gamma_{7,x}|^2}{|1 - \Gamma_s\Gamma_{3,x}|^2} \times \frac{(1 - |\Gamma_{3,s}|^2)}{\cos^2\zeta_7\,[1 - |\Gamma_x|^2 - 2\tan\zeta_7\, Im\Gamma_x]}\,. \tag{30}$$

We use $S_{ij}(N\text{-}M)$ to refer to the S-parameters between planes N and M, where N is considered the "first" plane; see eq (15).

Equations (28) and (30) can be used to determine the measured noise temperature on wafer, at plane 7. In our on-wafer tests, we also need to compute the noise temperature at plane 7 from a known noise temperature at plane 9 for the configuration of figure 4. This is easily done by using eqs (25) and (23) to write

$$T_7 = \alpha_{79}\,T_9 + [1 - \alpha_{79}]\,T_s\,, \tag{31}$$

with

$$\alpha_{79} = \frac{|S_{21}(9\text{-}7)|^2(1 - |\Gamma_s|^2)}{\cos^2\zeta_7\,|1 - \Gamma_s S_{11}(9\text{-}7)|^2[1 - |\Gamma_{7,s}|^2 - 2\tan\zeta_7\, Im\Gamma_{7,s}]}\,. \tag{32}$$

In this equation, the subscript s represents whatever source is connected at plane 9.

2.5 Use of "Pseudo-Waves"

The significant losses in typical on-wafer transmission lines mean that in general it is *not* a good approximation to take the characteristic impedance to be real. Therefore, the phase ζ is nonzero, and we should use the full, cumbersome, general forms for the mismatch factors, available power ratios, etc., as derived in the preceding section. Simplification is possible, however. Marks and Williams [15] have suggested and developed the use of what they call "pseudo-waves," which are linear combinations of the travelling waves, where the linear combination depends on the characteristic impedance and on a reference impedance of the user's choice. This transformation then induces a corresponding transformation of reflection coefficients and S-parameters at the reference plane(s) affected. The advantage of pseudo-waves is that if we choose a real reference impedance (typically 50 Ω), use of pseudo-waves and their associated reflection coefficients and S-parameters results in the familiar, lossless-line form for power, $|a|^2 (1-|\Gamma|^2)$. Consequently, ratios of powers, such as mismatch factors and available power ratios, also revert to their lossless-line forms. In fact, the travelling waves can be considered as just a special case of pseudo-waves, with reference impedance chosen to be the modal impedance of the travelling wave. Thus, the equations derived above for travelling waves also hold for pseudo-waves, provided that the ζ's are taken to be the phases of the reference impedances, and provided that all reflection coefficients and S-parameters are those appropriate to the reference impedance(s) chosen. (This may not be entirely obvious; it is proved in Appendix B.)

The price that one pays for the simplifications engendered by pseudo-waves is that the reflection coefficients and S-parameters must also be transformed to the reference impedance chosen. For reflection coefficients or S-parameters at reference planes in (nearly) lossless lines, this problem is absent since the characteristic impedance is real, to a good approximation. At reference planes on wafer, however, the characteristic impedance is complex, and $\zeta \neq 0$. If we use travelling waves, then we must use the phase of the modal impedance for ζ in the equations above. The reflection coefficients and S-parameters in that case are the "usual" ones defined for travelling waves. If we use pseudo-waves with $Z_{ref} = 50\ \Omega$, then we set $\zeta = \zeta_{ref} = 0$ in

the equations, but we must use pseudo-wave reflection coefficients and S-parameters for the on-wafer reference planes. Which choice is more convenient is determined to a large extent by the software used in making the on-wafer measurements. We shall use the NIST-developed package MultiCal® [21], with a multiline TRL calibration [22] to characterize the probes. One of the features of MultiCal is that it allows one to measure pseudo-wave quantities, and consequently we choose to use a reference impedance of 50 Ω and use the simplified ($\zeta = 0$) version of the equations. (MultiCal also provides for measurement of ζ, the phase of the characteristic impedance [23].) The form of the radiometer equation, eq (28), is unchanged, but eq (30) for the ratio of mismatch factors and available power ratios becomes

$$\frac{M_{0,s}\alpha_{03}}{M_{0,x}\alpha_{07}} = \frac{|S_{21}^{(50)}(3-0)|^2}{|S_{21}^{(50)}(7-0)|^2} \frac{|1-\Gamma_x^{(50)}\Gamma_{7,r}^{(50)}|^2}{|1-\Gamma_s^{(50)}\Gamma_{3,r}^{(50)}|^2} \frac{\left(1-|\Gamma_{3,s}^{(50)}|^2\right)}{\left(1-|\Gamma_x^{(50)}|^2\right)}, \qquad (33)$$

where the superscript "(50)" indicates that the reflection coefficient or S-parameter is with respect to a 50 Ω reference impedance. In computing the on-wafer noise temperature due to an off-wafer source, eq (31) remains the same, but eq (32), for the available power ratio, takes the form

$$\alpha_{79} = \frac{|S_{21}^{(50)}(9-7)|^2\left(1-|\Gamma_s^{(50)}|^2\right)}{|1-\Gamma_s^{(50)}S_{11}^{(50)}(9-7)|^2\left[1-|\Gamma_{7,s}^{(50)}|^2\right]}. \qquad (34)$$

If our on-wafer methods and software had measured only travelling-wave quantities, then it could be more convenient to use eq (30) as derived, with the measured travelling-wave reflection coefficients and S-parameters and the measured ζ.

3. THE EXPERIMENT

3.1 Experimental Setup

Figure 5 contains a block diagram of the general experimental setup, with relevant reference planes numbered. The radiometer is switched between the ambient standard noise source (plane 1), the nonambient standard noise

source (plane 3 or 6), and the on-wafer DUT (plane 7), measuring and recording the delivered power from each. The nonambient standard is usually the NIST cryogenic coaxial (GPC-7) primary standard [24], which is connected at plane 3. For some of the measurements, a previously calibrated, high-temperature check standard, connected at plane 6, is used as the nonambient standard. This is done when the cryogenic standard is being used elsewhere in the measurement or when we measure an on-wafer noise diode of very high noise temperature.

Detail of the detection system is shown in figure 6. It was originally built as a prototype of the 8 to 12 GHz detection section for the new radiometers discussed in the following paragraph. The design is similar to that in other NIST radiometers. The incident broadband noise power is amplified by the initial radio-frequency (rf) amplifier and then mixed with the signal from the local oscillator (LO). The output from the mixer is amplified and then filtered to pass frequencies within 5 MHz of 0. Thus the rf frequencies that contribute to the output power are in the range f = f(LO) ± 5 MHz. The output power is measured by a NIST type-IV power meter [25], and corrections are made for the effects of the filter shape. For reasons discussed below, the detection unit was designed and constructed to be *very* stable. Tests indicate that its output is stable within ±0.001 dB/12 h. The other critical feature of the detection unit is its linearity. The IF subsystem is the potential problem since it must handle the greatest power. The IF subsystem was tested and found to be linear within ±0.005 dB per 3 dB up to a power of 17 mW. Our typical measurements were done at IF powers less than 2 mW, and all measurements were kept well within the linear range. The internal ambient source shown in figure 6 is used for certain checks of the radiometer but not for noise measurements on a DUT.

The major difference between the radiometer of figures 5 and 6 and the "traditional" [13] NIST radiometers is the lack of a six-port reflectometer in the present system. All current NIST radiometers for 1 GHz and above include six-port reflectometers, which measure all relevant reflection coefficients for each measurement of a DUT. (Many separate measurements of the noise temperature are made at each frequency in calibrating a noise source.) A new generation of radiometers is being developed in conjunction with the

development of an amplifier noise-figure measurement capability [14]. These new systems will not have their own internal six-ports. Instead they will rely on an original set of measurements (plus periodic updates and checks) of the system reflection coefficients and path losses. This simplifies the radiometer and allows quicker calibrations, but it requires a high degree of stability and repeatability in the system.

Photographs of the measurement apparatus are shown in figures 7 and 8. If we begin with the closeup view of figure 7, the chuck on which the wafer rests during a measurement is located directly below the microscope. The probe to the right is probe 2, connected by a short section of semirigid cable to a bracket and GPC-7 connector. This connector corresponds to plane 9. In several of the measurements which used off-wafer sources to produce on-wafer noise, the noise source was connected at this plane. In the photograph, a cable is connected here. The other end of the cable, visible in figure 8, corresponds to plane 10 and is where the noise source was connected in the other tests using off-wafer sources. The cable is held securely, preventing any flexing during the course of the experiment. In figure 8, the structure to which the cable is secured is a jig, which was built to position the chuck and hence the wafer. This allowed probe 1, the left probe in the photographs, to remain fixed during the entire experiment, reducing the risk of changes in reflection coefficients and S-parameters to the left of plane 7. Probe 1 is connected by semirigid cable to the switch assembly, which is the light colored cylinder visible in figure 7. The switch assembly also houses the ambient standard, whose temperature is monitored by a thermistor. The connector emerging from the top of the switch assembly is port 6. The rectangular box connected to the axial (front) port of the switch is the detector unit. The connector emerging from the front of the detection unit, out of the page in figure 8, is the access port for plane 0, between the two isolators. The box and its contents are held at ambient temperature by the brass plate on top, with its water circulation. Ambient-temperature water is also circulated through the switch assembly. In figure 8 the cryogenic standard is the large, vertical, cylindrical canister below the switch, between the probe station and the instrumentation rack. The rack contains supporting electronics: the NIST type-IV power meter, a voltmeter to read the thermistors, the synthesizer, switch drivers, power supplies, filters, etc.

We do not circulate water through the probes or through the platform which supports the wafer. These elements could experience resistive heating, but for the power levels of this experiment we do not expect much effect. The most worrisome case was the on-wafer noise diode, which could heat up during use. To check this, we divided the run into halves and into thirds and checked for temperature change as a function of time. No significant difference was found. If the physical temperature of the diode is rising, it is not affecting the noise temperature. Another potential problem is that the temperature of the room is not as well regulated as the temperature of the circulating water. The two can differ by as much as about 2 K. We use "ambient" temperature to refer to the temperature of the ambient standard. The temperature of the circulating water is set for 296.0 K and is typically within about 0.1 K of the ambient-standard temperature. Consequently the switch assembly and the contents of the detector box are at ambient temperature. The wafer, the probes, and what we call "ambient" loads (which are not in water jackets) are at "room" temperature (in the absence of additional heating). This has little effect on the noise temperature measurements, but it does mean that the ambient loads in our tests are really "room temperature" loads, and consequently their noise temperatures may differ somewhat from ambient temperature.

We use the radiometer equation, eq (28), to compute the noise temperature T_x of the DUT from the delivered powers measured by the radiometer. Equation (33) is used for the ratio of mismatch factors and available-power ratios, requiring the measurement of the various reflection coefficients and S-parameters. The S-parameters and reflection coefficients which must be measured include $S_{21}(3\text{-}0)$, $S_{21}(7\text{-}0)$, Γ_x, $\Gamma_{7,r}$, Γ_S, $\Gamma_{3,r}$, and $\Gamma_{6,r}$. The two subscripts on some of the reflection coefficients refer to the reference plane and the direction, with r referring to the radiometer direction. S-parameters [$S_{ij}(2\text{-}0)$, $S_{ij}(3\text{-}0)$, $S_{ij}(6\text{-}0)$] from the switch ports through the switch to plane 0, between the two isolators, are measured with a VNA. In cases for which the reference plane occurs at a connector (planes 2, 3, 6, 9, 10), the reference plane is taken at the center of the connector, which is GPC-7 in all such cases. The radiometer has a port which allows access to plane 0. The reflection coefficients (Γ_S) of the cryogenic standard and the high-temperature check standard are also measured with the VNA. For

$\Gamma_{3,r}$ we use $\Gamma_{3,r} \approx S_{11}(3-0)$, and similarly $\Gamma_{6,r} \approx S_{11}(6-0)$. The accuracy of this approximation can be inferred from a comparison of $\Gamma_{7,r}$, which was measured, to $S_{11}(7-0)$, which can be constructed from the measured $S(7-2)$ and $S(2-0)$. This comparison indicates that the approximation should be accurate within 0.07 in the real and imaginary parts of $\Gamma_{3,r}$ and $\Gamma_{6,r}$ (0.1 in the magnitudes).

On-wafer quantities were measured using MultiCal [21]. An on-wafer multiline TRL calibration [22] was performed. The calibration kit consisted of a through, a reflect, and three transmission lines of different lengths, all of gold on a GaAs wafer. It was fabricated by the NIST High-Speed Microelectronics Project. In the calibration, the probes were defined to extend to the center of the through in the TRL calibration standards. The through is 0.50 mm long, and thus plane 7 is 0.25 mm from the probe-1 end of the through. Each probe thus includes a short (0.25 mm) section of coplanar waveguide (CPW), of which about 0.225 mm is between the probe tip and the reference plane, and 0.025 mm is behind the probe tip. In principle this length is chosen long enough to assure a single mode at planes 7 and 8. In practice we did not check for higher modes. The on-wafer calibration provides a measurement of $S_{ij}(7-2)$ and $S_{ij}(9-8)$. It also extends the VNA calibration to the reference planes 7 and 8 on wafer. The VNA and MultiCal can then be used to measure reflection coefficients at plane 7, both of the radiometer ($\Gamma_{7,r}$) and of the DUT (Γ_x). A number of different on-wafer DUT's were measured (discussed below), and for each the reflection coefficient was measured at plane 7. The S-parameters $S_{ij}(7-0)$ between planes 0 and 7 were not measured directly but were obtained by cascading $S_{ij}(7-2)$ and $S_{ij}(2-0)$.

In the course of the VNA and MultiCal measurements, a good deal of redundant information was obtained. We used this information to perform checks on our methods and measurements. For example, $\Gamma_{7,r}$, $\Gamma_{2,r}$, and $S(7-2)$ were all measured separately, but $\Gamma_{7,r}$ must equal the result of cascading $S(7-2)$ and $\Gamma_{2,r}$. A number of such checks were performed, and agreement was typically within a few percent. The probes were calibrated before and after the on-wafer measurements, and the largest difference in S_{21} for either probe was found to be 0.17 percent. The averages of several VNA measurements for the reflection coefficients of the primary standard and check standard were compared to results of independent measurements by personnel of the NIST Six-

Port Project at 8.0 GHz. The two agreed within ±0.001. It was also found that the magnitudes of S_{21} for the three switch ports were equal within about 0.1 dB. They need not have been equal, since we correct for any difference, but it is reassuring that they are. A number of other repeatability checks were performed, with similar results. These checks give us confidence that we are correctly measuring the reflection coefficients and S-parameters.

3.2 Noise Sources

The principal purpose of the experiment was to test our ability to measure noise temperature on wafer. In addition, we wanted to resolve two specific questions which had arisen in preliminary measurements. One was whether any (nonambient) radiation was entering the system through the open, on-wafer transmission line, thereby adding additional power to the lines and corrupting the noise measurements. The other issue was whether flexible cables could be used to connect off-wafer sources to one of the probes and thus to a transmission line on wafer. The cables would have to be disconnected and reconnected in order to measure their characteristics and then to use them in the noise measurements. Earlier tests had suggested that this process could introduce variations as large as about 12 percent in the noise- temperature measurement, which was considerably larger than we were willing to tolerate.

To address these questions, we measured a number of different noise sources. We began by measuring a high-temperature check standard which had previously been measured at 8 GHz on our coaxial noise-temperature calibration system. This standard was measured at port 6, in figure 5, which is not on wafer. Measurement of its noise temperature tells us nothing about our on-wafer capabilities but does provide a check that the new radiometer and the associated computations are functioning properly.

The simplest on-wafer noise source was just a resistor on a GaAs wafer. The leads from the resistor are the same as the CPW line used in the on-wafer calibration kit. Reference plane 7, at which we measure the noise temperature, is therefore a distance 0.25 mm from the end of the CPW (about 0.225 mm from the tip of the probe), as discussed near the end of section 3.1.

Since the resistor is at the same (room) temperature as the line, the exact location of the reference plane is not especially important in this measurement, but in other measurements it is critical. The resistor is in equilibrium with its surroundings, at room temperature. As discussed above, room temperature may not be exactly "ambient" temperature, but it is close (within about 2 K). Measurement of the resistor's noise temperature constitutes a (not very demanding) test of the measurement methods and system. It also provides a test of whether outside radiation is entering the system. If the resistor and transmission line are absorbing (nonambient) radiation from the surrounding environment, then the measured noise temperature will differ from the room or ambient temperature. Preliminary measurements indicated that a nearby incandescent lamp could affect the measured noise temperature. Such obvious local sources were removed, but there were still the fluorescent room lights, emissions from equipment in the room, and various external sources -- the room is shielded, but not very well.

The second on-wafer source was a noise diode bonded to a short section of CPW line on a GaAs wafer, with no attenuating circuit to control its reflection coefficient. The on-wafer configuration is shown in figure 9. Bias for the diode was supplied through probe 1 from a monitored current source. The section of CPW to the left of plane 7 is the same as that used in the calibration kit, and therefore the on-wafer calibration and characterization of probe 1 is still applicable. Two problems render this diode source less than ideal. The lack of an attenuator means that its reflection coefficient will probably not be very well matched to the line or probe and that it may exhibit rather erratic behavior as a function of frequency. In addition, the noise temperature of the diode is not known by some independent means. We therefore have no way of checking that the answer we obtain is correct. Nevertheless, the exercise should provide practice and may uncover difficulties in handling a source with very high noise temperature.

Because the diode is not a linear device, its reflection coefficient may depend on the incident power. In measuring its noise temperature, we are interested in its reflection coefficient (Γ_D) for very low power. We measured Γ_D for three different values of incident power, including the lowest

allowed by our VNA. The power levels from the synthesizer of the VNA were −9 dB, −10 dB, and −11 dB, all relative to 1 mW. The corresponding powers incident on the diode were roughly 11 dB lower. We found that Γ_D varied little over the range measured, and was unchanged within measurement accuracy between the two lowest powers. Consequently, the value at the lowest power should be valid for the incident powers encountered in the noise temperature measurement. The noise powers encountered are far smaller than the VNA test levels. Noise is broadband, but even using a 1 GHz bandwidth the available powers from sources with noise temperatures of 10^2 K, 10^4 K, and 10^6 K are −88.6 dB, −68.6 dB, and −48.6 dB, all relative to 1 mW.

In order to properly test our ability to measure noise temperature on wafer, we need on-wafer, nonambient (preferably both high-temperature and low-temperature) noise sources with known noise temperatures. These are not available, and so we produced known noise temperatures on wafer by using known off-wafer noise sources. The configuration is shown in figure 10(a). A check standard with known noise temperature was connected to probe 2 at plane 9, and probe 2 was then connected to an on-wafer transmission line at plane 8. The transmission line was one of those in the calibration kit mentioned in Section 3.1; both the through and the longest line (6.565 mm between planes 7 and 8) of the kit were used. Since the properties of probe 2 were determined by the on-wafer calibration, and since the properties of the through and the line are known, we can use eqs (31) and (34) to calculate the noise temperature at plane 7 on wafer in terms of the known noise temperature at plane 9. The calculated value can then be compared to the measurement result. We also connected an ambient source at plane 9, with both the line and the through on wafer, and measured the resulting noise temperatures at plane 7. The cryogenic primary standard must remain vertical, and therefore it cannot be connected directly to plane 9. It was connected by a flexible cable, with the connection between the cable and standard being labelled as plane 10, as in figure 10(b). The check standard was also attached at plane 10. For both cases both the through and the line were used on wafer, and the noise temperature at plane 7 was calculated and measured in each case. In measurements with the cable, great care was taken to minimize any movement or flexing of the cable between the time its properties were measured on the VNA and the time of the measurement of the noise temperatures.

To facilitate discussion of the various measurement configurations, we introduce some additional notation. Each configuration will be labeled by the plane at which the noise temperature was measured and what was connected at that plane. We will use Cr to denote the cryogenic primary standard, Ck for the check standard, A for an ambient load, R for the on-wafer resistor, D for the on-wafer noise diode, L for the on-wafer calibration-kit line, T for the on-wafer calibration-kit through, and the respective number for each reference plane. Thus the measurement of the check standard at port 6 in figure 5 is referred to as 6Ck; the measurements of the on-wafer diode and resistor are 7D and 7R respectively; the ambient load connected at plane 9 with the line on wafer is 7L9A; the cryogenic primary standard connected through the cable with the through on wafer is 7T10Cr; etc.

To summarize, we measured a variety of noise sources, providing a range of significant tests of our ability to measure noise temperature on wafer. The direct measurement of the check standard (6Ck) tested the off-wafer aspects of the system, including the radiometer, the switch assembly, and a portion of the data-analysis software. The on-wafer noise diode measurement (7D) allowed us to measure an unknown noise source with very high noise temperature (nearly 10^6 K). It tested whether we could get *an* answer for such a device, but we do not know what the correct answer is. The three measurements of ambient loads (7R, 7T9A, and 7L9A) provided a test of our ability to measure a known noise temperature, albeit a rather easy one since measurement of an ambient load is insensitive to some common errors. Since the ambient measurements involve three different on-wafer configurations, they do provide a very good test of whether any (nonambient) outside radiation is getting into the system. The remaining six noise-temperature measurements are a good test of our entire system and methods. The two using the cryogenic primary standard (7T10Cr, 7L10Cr) test our ability to measure low noise temperatures (about 160 K and 180 K) on wafer, and the four using the check standard (7T9Ck, 7L9Ck, 7T10Ck, 7L10Ck) test our ability to measure high temperatures (about 5000 K to 7600 K). The fact that we measure the check standard both when it is connected directly to probe 2 at plane 9 and when it is connected to the cable at plane 10 enables us to isolate any problems introduced by the flexible cable.

3.3 Results

Measurements were made from 7.8 GHz to 8.2 GHz in increments of 0.1 GHz. These frequencies were chosen in order to compare to earlier, preliminary measurements. We intend to expand the frequency range in future tests. The first test performed was the direct measurement of the noise temperature of the check standard (6Ck). The results of these measurements were compared to results of previous measurements of the same device using the present system and to an earlier measurement using the traditional NIST radiometer which is used for official calibrations. The agreement was excellent. The present result at 8.0 GHz differs from the calibration-system result by 4 K, out of 9238 K (0.04 percent). The two sets of measurements on the present system differed by at most 0.15 percent. We conclude that the radiometer is functioning properly for off-wafer measurements and that its repeatability is very good.

The results of the measurements on the ambient loads (7R, 7T9A, and 7L9A) are shown in figure 11. The agreement between the measured noise temperature and the ambient temperature is very good in all three cases. The fractional difference between measured and ambient temperatures,

$$\Delta \equiv 2\,\frac{T(measured) - T(predicted)}{T(measured) + T(predicted)}\,, \qquad (35)$$

is plotted in figure 12, where the predicted noise temperature is the ambient temperature in this case. The measured noise temperature is consistently about 0.5 percent (1.5 K) above the ambient temperature. As discussed in section 3.1, even this small discrepancy can be attributed to the fact that the sources being measured are at "room" rather than "ambient" temperature, and the two can differ by as much as 2 K. We therefore conclude that our system and methods correctly measure on-wafer noise temperatures near ambient. Because the three ambient loads measured correspond to three different configurations on wafer (resistor, through, line), the fact that none of the three exhibits signs of external radiation effects is a strong indication that such effects are absent in our on-wafer noise measurements.

Figure 13 contains the results for the two sets of measurements for which the high-temperature check standard was connected to probe 2 at plane 9. For both the through (7T9Ck) and the line (7L9Ck) on wafer, the noise temperature was measured at plane 7. The predicted results in figure 13 are the noise temperatures at plane 7 calculated from the known noise temperature of the check standard and the measured properties of probe 2 (or probe 2 plus line) using eqs (31) and (34). The agreement between measured and predicted noise temperatures is good in both cases, around 0.5 percent for 7T9Ck and around 1 percent for 7L9Ck. The largest difference, at 8.2 GHz in 7L9Ck, is 110 K (1.75 percent). To put this in perspective, a typical expanded (2σ) uncertainty in our coaxial noise-temperature calibrations is 1.0 percent to 1.5 percent. (The uncertainty analysis for the present experiment is presented in the next subsection.) Results for the measurements with the check standard connected to probe 2 through a cable (7T10Ck and 7L10Ck) are presented in figure 14. The agreement between measurement and predicted noise temperatures is good for 7L10Ck (around 1.5 percent) but somewhat worse for 7T10Ck (around 2.2 percent). The results for the cryogenic standard, attached through a cable to probe 2 (7T10Cr and 7L10Cr) are presented in figure 15. Agreement between measurement and prediction is again good, around 1 percent for most frequencies, though it is about 2 percent and 2.5 percent at 8.2 GHz. The comparison of measurement and prediction for nonambient, on-wafer noise temperatures is summarized in figure 16, which plots the Δ of eq (35) for each of the six known nonambient temperatures we measured. Most of the points lie in the $|\Delta| \leq 2$ percent range, with a few between 2.0 percent and 2.6 percent.

Finally, in figure 17, we show the noise temperature measured for the on-wafer noise diode. As we discussed above, we do not know the diode's noise temperature from other information. The measurement indicates that the noise temperature of the diode is very high, approaching 10^6 K. In order not to saturate the radiometer, an attenuator was introduced in front of it, between plane 2 and the first isolator. This in turn lowered the power from the cryogenic standard unacceptably, and so the previously measured high-temperature check standard was used as the nonambient standard in this measurement.

3.4 Uncertainty Analysis and Checks

To assess the significance of the differences between measurement and prediction in the preceding section, we need to estimate the uncertainties in both the measured and the predicted values. We must also consider the correlation between possible errors in measurement and prediction. The comparison we performed magnifies some potential errors and is insensitive to others. We will first present an uncertainty analysis for our measurements of noise temperature on wafer. The analysis will hardly be definitive, but will be sufficient to judge the significance of the observed differences between experiment and theory. We will then consider uncertainties in the predictions and in the Δ defined by eq (35).

The noise temperature of the DUT is calculated from eq (28), with $(\Delta T_x)_{is}$ neglected,

$$T_x = T_a + (T_s - T_a)\,\frac{M_{0,s}\,\alpha_{03}}{M_{0,x}\,\alpha_{07}}\,\frac{Y_x - 1}{Y_s - 1}\,. \tag{36}$$

This form assumes a perfect isolator as well as a linear radiometer. Uncertainties in T_x arise due to uncertainties in the determination of the quantities appearing on the right side of eq (36) and due to departures from perfect isolation and linearity. For the present analysis, we will be concerned with the uncertainties arising in a single measurement of T_x. In keeping with the notation of the ISO [26,27], we will use u_{Tx} to denote the standard uncertainty in the measurement of T_x. We shall deal primarily with type-B uncertainties; type-A uncertainties arise in measurement of the powers, but enough samples are taken that these uncertainties are negligible in the present experiment. We use $\mathscr{E}_z$ to denote the fractional standard uncertainty in the parameter z, for example, $\mathscr{E}_{Cry} \equiv u_{TCry}/T_{Cry}$.

The uncertainty in the noise temperature of the cryogenic standard contributes to the uncertainty in T_x as

$$\frac{u_{T_x}(Cry)}{T_x} = \left|1 - \frac{T_a}{T_x}\right| \left|\frac{T_S}{T_a - T_S}\right| \mathscr{E}_{Cry}\,. \tag{37}$$

The fractional uncertainty in the GPC-7 cryogenic standard which was used in all the measurements (except of the on-wafer diode) is about 1 percent at 8 GHz. This results in an uncertainty of roughly 0.35 percent in T_x for T_x much larger than T_a.

The contribution of the uncertainty in the ambient standard temperature to the uncertainty in the DUT noise temperature is given by

$$\frac{u_{T_x}(Amb)}{T_x} = \left|\frac{T_x - T_s}{T_a - T_s}\right| \frac{T_a}{T_x} \mathscr{E}_{T_a} . \qquad (38)$$

The uncertainty in the ambient temperature is $u_{Ta} = 0.1$ K. Since the ambient temperature is kept at 296 K, this results in $\mathscr{E}_{Ta} = 0.034$ percent. The type-A uncertainty in the ambient temperature measurement was evaluated in one of the tests. It was found to be 0.015 K, or 0.005 percent, and was therefore assumed negligible in all the measurements. The ambient-temperature contribution to u_{Tx} is negligible for most values of T_x, but it survives near $T_x = T_a$, where the other uncertainties vanish.

The uncertainty in the power ratio measurements (Y_S and Y_x) was evaluated in reference [28], where it was found to be negligible. A similar analysis in the present case results in $\mathscr{E}_Y \leq 0.05$ percent, which can be safely neglected. The linearity of the detection unit of the radiometer was discussed in subsection 3.1. The powers involved in the present measurements are less than 2.5 mW. Any error due to radiometer nonlinearity for these powers is negligible. The uncertainty due to finite (40 dB) isolation can be evaluated following the calculation in reference [13], with appropriate changes for 40 dB isolation rather than the 50 dB assumed there. This leads to an uncertainty in T_x of about 0.1 percent for small values of T_x and much less for large values of T_x. We neglect this contribution to u_{Tx}.

The final contribution to u_{Tx} is due to uncertainties in the measurement of the various S-parameters and reflection coefficients which appear in the expression for $(M_{0,S}\alpha_{03}) / (M_{0,x}\alpha_{07})$, eq (33). If we use $\mathfrak{R}$ to denote this ratio of $M\alpha$'s, and compute the variation in $\mathfrak{R}$ due to small variations in the S-parameters and reflection coefficients, we obtain

$$\frac{\delta \Re}{\Re} = 2\left(\frac{\delta |S_{21}(3-0)|}{|S_{21}(3-0)|} + \frac{\delta |S_{21}(7-0)|}{|S_{21}(7-0)|}\right) + D_\Gamma . \qquad (39)$$

D_Γ is a rather lengthy expression containing variations in the reflection coefficients. Each of the terms in D_Γ is of the form $g \times |\Gamma_i \Gamma_j| \times \mathscr{E}_\Gamma$, where g is of order 1, Γ_i and Γ_j are reflection coefficients each of whose magnitudes is of order 0.1, and $\mathscr{E}_\Gamma$ is the fractional uncertainty in measuring either the magnitude or phase of a reflection coefficient. For typical values of $\mathscr{E}_\Gamma$, D_Γ is less than about 0.1 percent and can be neglected, so that

$$\frac{\delta \Re}{\Re} \approx 2\left(\frac{\delta |S_{21}(3-0)|}{|S_{21}(3-0)|} + \frac{\delta |S_{21}(7-0)|}{|S_{21}(7-0)|}\right), \qquad (40)$$

which in turn leads to

$$\frac{u_{T_x}(\Re)}{\Re} \approx 2\left|1 - \frac{T_a}{T_x}\right| \sqrt{\frac{u^2_{|S_{21}(3-0)|}}{|S_{21}(3-0)|^2} + \frac{u^2_{|S_{21}(7-0)|}}{|S_{21}(7-0)|^2}} . \qquad (41)$$

The magnitude of $S_{21}(3-0)$ is determined by a coaxial VNA measurement. From the manufacturer's specifications, the fractional uncertainty in this measurement is

$$\frac{u_{|S_{21}(3-0)|}}{|S_{21}(3-0)|} \approx 0.19\% . \qquad (42)$$

$S(7-0)$ is formed by cascading $S(7-2)$ and $S(2-0)$. The uncertainty which results is

$$\frac{u^2_{|S_{21}(7-0)|}}{|S_{21}(7-0)|^2} \approx \frac{u^2_{|S_{21}(7-2)|}}{|S_{21}(7-2)|^2} + \frac{u^2_{|S_{21}(2-0)|}}{|S_{21}(2-0)|^2} . \qquad (43)$$

The fractional uncertainty in the magnitude of $S_{21}(2-0)$ is the same as that for $S_{21}(3-0)$, 0.19 percent. The uncertainty in the magnitude of $S_{21}(7-2)$ is somewhat more problematic. Repeatability of such measurements was checked both with the Verify feature of the MultiCal program and by comparing results of repeat measurements. This led to a type-A uncertainty of 0.2 percent in

the magnitude of $S_{21}(7\text{–}2)$. The type–B uncertainty has two components, one due to the VNA measurements and the other due to the on–wafer calibration. Using the manufacturer's specifications for the VNA uncertainty and typical values for $S_{21}(7\text{–}2)$ and $S_{21}(9\text{–}8)$, we obtain a fractional uncertainty in $|S_{21}(7\text{–}2)|$ due to the VNA measurements of 0.15 percent, The uncertainty due to the on–wafer calibration (imperfect calibration standards, etc.) is difficult to assess. We estimate that it is double the uncertainty in the VNA measurements and use $u(\text{o–w cal}) \approx 0.003$, $u(\text{o–w cal})/|S_{21}(7\text{–}2)| \approx 0.4$ percent. Combining the various (independent) components of the uncertainty, we obtain for the fractional uncertainty in $|S_{21}(7\text{–}2)|$,

$$\frac{u_{|S_{21}(7-2)|}}{|S_{21}(7-2)|} \approx \sqrt{0.002^2 + 0.0015^2 + 0.0040^2} = 0.0047 . \qquad (44)$$

Equation (43) then yields a fractional uncertainty in $|S_{21}(7\text{–}0)|$ of 0.51 percent, and eq (41) for the fractional uncertainty in the ratio of mismatch factors and α's becomes

$$\frac{u_{T_x}(\Re)}{T_x} \approx 0.011 \times \left| 1 - \frac{T_a}{T_x} \right| . \qquad (45)$$

Our estimate for the standard uncertainty in the measurement of T_x is then

$$\frac{u_{T_x}}{T_x} = \sqrt{\frac{u_{T_x}^2(Cry)}{T_x^2} + \frac{u_{T_x}^2(Amb)}{T_x^2} + \frac{u_{T_x}^2(\Re)}{T_x^2}} , \qquad (46)$$

with the individual components given by eqs (37), (38), and (45). This result is plotted as a function of DUT noise temperature in figure 18, with the fractional uncertainty given in figure 18(a) and the standard uncertainty given in figure 18(b). For DUT noise temperatures down to about 150 K, the uncertainty is below about 1.1 percent. For comparison, a typical standard uncertainty for our calibrations of coaxial noise sources is about 0.6 percent or 0.7 percent at this frequency. The dominant component of the uncertainty is $u_{Tx}(\Re)$, which by itself accounts for an uncertainty of about 1 percent in the DUT noise temperature (for large T_x). It is unfortunate that this dominant component is also the one which is most approximate, due to our ignorance of

the uncertainty in the on-wafer calibration. Our uncertainty estimate is therefore quite tentative at this time, although we do have evidence that it is not too wrong, as discussed below.

In comparing measured to predicted on-wafer noise temperatures, we also must take into account the uncertainty in the predictions. The predicted noise temperature is calculated from eq (31), where plane 9 is replaced by plane 10 when the cable is used. The two principal sources of uncertainty are in T_9, the noise temperature of the known source which is connected at plane 9 (or 10), and in α_{79}, the available power ratio between planes 7 and 9 (or 10). Denoting uncertainties due to these two sources as $u_{Tx}(T_9)$ and $u_{Tx}(\alpha)$, we have

$$\frac{u_{T_x}(\alpha)}{T_x} \approx \left|1 - \frac{T_a}{T_7}\right| 2 \frac{u_{|S_{21}(9-7)|}}{|S_{21}(9-7)|} \approx \left|1 - \frac{T_a}{T_7}\right| \times 0.9\%, \qquad (47)$$

and

$$\frac{u_{T_7}(T_9)}{T_7} = \left|1 - (1 - \alpha_{79}) \frac{T_a}{T_7}\right| \frac{u_{T_9}}{T_9} \approx \left|1 - (1 - \alpha_{79}) \frac{T_a}{T_7}\right| \times 0.6\%. \qquad (48)$$

Combining the two in quadrature leads to a fractional uncertainty in the calculated value of T_7 of about 0.8 percent for the low values of T_7 and about 1.1 percent for large T_7.

These numbers are not directly applicable to the difference between measurement and prediction, however, because the uncertainties in measured and predicted noise temperatures are highly correlated. In the case of $u_{Tx}(T_9)$, the correlation is due to the fact that the known noise temperature of the source which is attached at plane 9 was determined by comparing it to the same primary standard which is being used in the present measurement. In computing Δ from eq (35), any error in the measurement of the noise temperature of the source at plane 9 cancels insofar as it is repeatable. Only the nonrepeatable part of the comparison of the two sources contributes to Δ, and that is small. For the contribution of the uncertainty in α_{79}, there is the question of correlation between uncertainties in α_{79} and in α_{27}, or between uncertainties in $|S_{21}(7-9)|$ and those in $|S_{21}(2-7)|$. In the characterization of the probes, an error could be made in measuring the product of $|S_{21}(7-9)|$ and $|S_{21}(2-7)|$ or

in separating the product into the two factors. An uncertainty in the product leads to a positive correlation between the two uncertainties and a negative correlation between the uncertainties in the measured and predicted values for T_7. Such uncertainties would then add linearly in the uncertainty in Δ, which measures the difference between measured and predicted values. Conversely, any error in separating the product of $|S_{21}(7-9)|$ and $|S_{21}(2-7)|$ into the two factors would cancel in forming Δ. Given our relative ignorance of the uncertainties the on-wafer calibration, we cannot make an informed judgement regarding the correlation.

To summarize the uncertainty results, the uncertainty in the measured noise temperatures on wafer is about 0.9 percent for the two low noise temperatures and about 1.1 percent for the high noise temperatures. The relevant part of the uncertainty in the predictions is about 0.8 percent for the two low noise temperatures and about 0.9 percent for high noise temperature. The uncertainties in measurement and prediction may be highly correlated, and therefore the uncertainty in Δ can be as large as about 1.7 percent for low noise temperature and about 2 percent for high noise temperature. All these uncertainties correspond approximately to 1σ. For a 95 percent confidence level (2σ), we would double all the values. We return then to the discrepancies between measurement and theory, the Δ plotted in figure 16. For the high noise temperatures (7T9Ck, 7L9Ck, 7T10Ck, and 7L10Ck), $|\Delta| \leq 2.5$ percent. This is consistent with the estimated uncertainties. For the low temperatures, $|\Delta| \leq 2.1$ percent except for one point, where $|\Delta| = 2.56$ percent. This also is consistent with the estimated uncertainties, provided that the uncertainties in measurement and prediction are correlated. We conclude that our measurement results agree with the predictions as well as should be expected. We also regard the agreement as an indication that our estimate of the uncertainty is not grossly wrong.

4. SUMMARY AND DISCUSSION

The core of this paper comprised theoretical and experimental sections. The theoretical section presented the theoretical background and developed the formalism necessary for the analysis of noise-temperature measurements on wafer. The relevant equations were derived, including the radiometer equation

and expressions for the mismatch factors and available-power ratios. In general these equations differ from the usual ones due to the presence of significant loss in the on-wafer transmission lines. The equations can be transformed into the traditional forms at the expense of using transformed ("pseudo-wave") reflection coefficients and S-parameters. The software we used for our on-wafer measurements [21] provided these transformed quantities, and consequently we used the transformed versions of the equations. The general versions of all equations were also presented, however.

The experimental portion of the paper reported a series of measurements performed to test our ability to accurately measure noise temperature on wafer. The experimental setup was presented, and the procedures were outlined. Several different configurations were used to produce known on-wafer noise temperatures, which were then measured and compared to the predicted values. Different ambient sources on wafer allowed us to test for the effect of outside radiation. Several measurements through a flexible cable permitted us to test for its effects as well. An on-wafer noise diode with very high noise temperature (nearly 10^6 K) was also measured. The uncertainties in the noise-temperature measurements were estimated.

The tests confirm both that we can measure noise temperature on wafer and that we can produce known on-wafer noise temperatures using off-wafer sources. Measurements of ambient loads agreed with room temperature to within about 0.5 percent, which is less than the uncertainty in the room temperature. Any effect of outside radiation entering the system was negligible. Results for nonambient noise temperatures agreed with predictions to within the estimated expanded ($k = 2$) uncertainty. The estimate of the standard uncertainty was 1.1 percent and below for noise temperatures above about 150 K. For lower noise temperatures, the *fractional* uncertainty increased, but the standard uncertainty remained below 3.5 K. Performing measurements through a flexible cable did not degrade the accuracy noticeably, provided that great care was taken to minimize movement of the cable during the course of the experiment. All measurements on wafer were performed using old probes with appreciable loss (about 1.5 dB). Future measurements will use newer, less lossy probes, resulting in a slight decrease in the uncertainty.

While successful, the tests did have limitations. Only a narrow band of frequencies was measured (7.8 GHz to 8.2 GHz). In addition, our comparison of measured and predicted results was insensitive to certain errors in the measurement of the S-parameters of the probes. The tests were sensitive to the product of the available-power ratios of the two probes, but not to the available-power ratio of either probe individually. These points constitute significant shortcomings of the set of tests described in this paper, shortcomings which will be remedied in future experiments.

I am very grateful to R. Billinger and J. Rice for performing the measurements. I also thank D. F. Wait for valuable comments and assistance in designing the experiment, D. Williams and D. Walker for extensive help in using MultiCal for on-wafer measurements, and L. Dunleavy of the University of South Florida for comments and suggestions on the manuscript. This work was supported in part by the NIST/Industrial MMIC Consortium.

5. REFERENCES

[1] Gupta, M.S.; Pitzalis, O.; Rosenbaum, S.E.; Greiling, P.T. Microwave noise characterization of GaAs MESFET's: Evaluation by on-wafer low-frequency output of noise current measurement. IEEE Trans. Microwave Theory Tech. MTT-35(12): 1208-1218; 1987 December.

[2] Davidson, A.C.; Leake, B.W.; Strid, E. Accuracy improvements in microwave noise parameter measurements. IEEE Trans. Microwave Theory Tech. MTT-37(12): 1973-1978; 1989 December.

[3] Adamian, V. 2-26.5 GHz on-wafer noise and S-parameter measurements using a solid state tuner. 34th ARFTG Conference Digest; Ft. Lauderdale, FL, 1989. 33-40.

[4] Dunleavy, L. A Ka-band on-wafer s-parameter and noise figure measurement system. 34th ARFTG Conference Digest; Ft. Lauderdale, FL; 1989. 127-137.

[5] Hughes, B.; Tasker, P. Improvements to on-wafer noise parameter measurements. 36th ARFTG Conference Digest; Monterrey, CA; 1990. 16-25.

[6] Woodin, C.; Wandrei, D.; Adamian, V. Accuracy improvements to on-wafer amplifier noise figure measurements. 38th ARFTG Conference Digest; San Diego, CA; 1991, 129-138.

[7] Dambrine, G.; Happy, H.; Danneville, F.; Cappy, A. A new method for on wafer noise measurement. IEEE Trans. Microwave Theory Tech. MTT-41(3): 375-381; 1993 March.

[8] Caddemi, A.; Sannino, M. Comparison between complete and simplified methods for determining the microwave noise parameters of HEMTs. 43th ARFTG Conference Digest; San Diego, CA; 1994. 121-126.

[9] Fenton, J.R. Noise parameter data comparison while varying the on-wafer S-parameter calibration technique. 44th ARFTG Conference Digest; Boulder, CO; 1994. 89-97.

[10] Boudiaf, A.; Dubon-Chevallier, C.; Pasquet, D. Verification of on-wafer noise parameter measurements. IEEE Trans. Instrum. Meas. IM-44(2): 332-335; 1995 April.

[11] Boudiaf, A.; Scavennec, A. Experimental investigation of on-wafer noise parameter measurement accuracy. 1996 IEEE MTT-S International Microwave Symposium Digest, Vol. 3; San Francisco, CA; 1996. 1277-1280.

[12] Miller, C.K.S.; Daywitt, W.C.; Arthur, M.G. Noise standards, measurements, and receiver noise definitions. Proc. IEEE, 55(6): 865-877; 1967 June.

[13] Daywitt, W.C. Radiometer equation and analysis of systematic errors for the NIST automated radiometers. Natl. Inst. Stand. Technol. Tech. Note 1327; 1989 March.

[14] Wait, D.F.; Randa, J. Amplifier noise measurements at NIST. IEEE Trans. Instrum. Meas., to be published; 1997 April.

[15] Marks, R.; Williams, D. A general waveguide circuit theory. J. Res. Natl. Inst. Stand. Technol. 97(5): 533–562; 1992 September–October.

[16] Collin, R.E. Foundations for Microwave Engineering. New York: McGraw–Hill; 1992. Ch. 3, 4.

[17] Ramo, S.; Whinnery, J.R.; Van Duzer, T. Fields and Waves in Communications Electronics. New York: Wiley; 1984. Ch. 5, 8.

[18] Marcuvitz, N. Waveguide Handbook. New York: McGraw–Hill; 1951; and London: Peter Peregrinus; 1986. Ch. 1.

[19] Jordan, E.; Balmain, K. Electromagnetic Waves and Radiating Systems, 2nd ed. Englewood Cliffs, NJ: Prentice Hall; 1968. Ch. 7.08.

[20] Wait, D.F. Thermal noise from a passive linear multiport. IEEE Trans. Microwave Theory Tech. MTT–16(9): 687–691; 1968 September.

[21] Marks, R.; Williams, D. NIST/Industrial MMIC Consortium Software Manuals. 1992 February.

[22] Marks, R. A multiline method of network analyzer calibration. IEEE Trans. Microwave Theory Tech. MTT–39(7): 1205–1215; 1991 July.

[23] Marks, R.; Williams, D. Characteristic impedance determination using propagation constant measurement. IEEE Microwave & Guided Wave Lett. 1(6): 141–143; 1991 June.

[24] Daywitt, W.C. A coaxial noise standard for the 1 GHz to 12.4 GHz frequency range. Nat. Bur. Stands. (U.S.) Tech. Note 1074; 1984 March.

[25] Larsen, N.T. A new self–balancing DC–substitution RF power meter. IEEE Trans. Instrum. Meas. IM–25(4); 343–347; 1976 December.

[26] ISO. Guide to the Expression of Uncertainty in Measurement. International Organization for Standardization; Geneva, Switzerland; 1993.

[27] Taylor, B.N.; Kuyatt, C.E. Guidelines for evaluating and expressing the uncertainty of NIST measurement results. Natl. Inst. Stand. Technol. Tech. Note 1297, 1994 edition; 1994 September.

[28] Pucic, S.P. The uncertainty in Y-factor measurements. URSI National Radio Science Meeting Digest; Boulder, CO; 1995. 39.

APPENDIX A

It is instructive, though tedious, to derive eq (25) explicitly from the travelling wave amplitudes, S-parameters, and reflection coefficients. To do so we use eq (13) for the available power at plane 2, using $\hat{b}_{GS}$ from eq (17) for the amplitude of the generator wave. We obtain

$$P_2^{avail} = \left|\frac{S_{21}}{1-\Gamma_G S_{11}}\right|^2 \frac{\left|\hat{b}_G + \Gamma_G \hat{b}_1 + \frac{1-\Gamma_G S_{11}}{S_{21}}\hat{b}_2\right|^2}{\left[1-|\Gamma_{GS}|^2 - 2\,Im\Gamma_{GS}\tan\zeta_2\right]\cos^2\zeta_2}\,, \tag{A1}$$

where it is understood that we wish to average the entire expression over time. When the expression involving the wave amplitudes is expanded and averaged over time, it yields terms proportional to $|\hat{b}_G|^2$, $|\hat{b}_1|^2$, $|\hat{b}_2|^2$, and $Re(\hat{b}_1\hat{b}_2^*)$. By using eqs (14), (22), and (23), we can rewrite the term proportional to $|\hat{b}_G|^2$ as

$$\left|\frac{S_{21}}{1-\Gamma_G S_{11}}\right|^2 \frac{\langle|\hat{b}_G|^2\rangle}{\left[1-|\Gamma_{GS}|^2 - 2\,Im\Gamma_{GS}\tan\zeta_2\right]\cos^2\zeta_2} \tag{A2}$$

$$= \alpha_{21} P_1^{avail} = \alpha_{21} k_B B T_G\,.$$

That accounts for the first term in eq (25). That's the easy part. The remaining piece requires more work. First expand the remaining part of the numerator of eq (A1), and use eqs (18), (19), and (20) to eliminate the wave amplitudes,

$$\left\langle \left| \Gamma_G \hat{b}_1 + \frac{1 - \Gamma_G S_{11}}{S_{21}} \hat{b}_2 \right|^2 \right\rangle =$$

$$|\Gamma_G|^2 [(1 - |S_{11}|^2 - 2\tan\zeta_1 \, Im S_{11}) \cos^2\zeta_1 - |S_{12}|^2 \cos^2\zeta_2] \, P_A$$

$$+ \frac{|1 - \Gamma_G S_{11}|^2}{|S_{21}|^2} [(1 - |S_{22}|^2 - 2\tan\zeta_2 \, Im S_{22}) \cos^2\zeta_2 - |S_{21}|^2 \cos^2\zeta_1] \, P_A$$

$$- 2\,Re\left(\frac{\Gamma_G (1 - \Gamma_G S_{11})^*}{S_{21}^*} [S_{21}^* (S_{11} + j\tan\zeta_1) \cos^2\zeta_1 \right.$$

$$\left. + S_{12} (S_{22}^* - j\tan\zeta_2) \cos^2\zeta_2] \right) P_A \,, \qquad \text{(A3)}$$

$$P_A \equiv k_B B T_A \,.$$

By regrouping terms proportional to $\cos^2\zeta_1$ and $\cos^2\zeta_2$, we get

$$\left| \frac{S_{21}}{1 - \Gamma_G S_{11}} \right|^2 \left\langle \left| \Gamma_G \hat{b}_1 + \frac{1 - \Gamma_G S_{11}}{S_{21}} \hat{b}_2 \right|^2 \right\rangle = [X_1 \cos^2\zeta_1 + X_2 \cos^2\zeta_2] \, P_A \,, \qquad \text{(A4)}$$

where

$$X_1 = |S_{21}|^2 \left[\frac{|\Gamma_G|^2 \, [1 - |S_{11}|^2 - 2\tan\zeta_1 \, Im S_{11}]}{|1 - \Gamma_G S_{11}|^2} - 1 \right.$$

$$\left. - 2\,Re\left(\frac{\Gamma_G (S_{11} + j\tan\zeta_1)}{(1 - \Gamma_G S_{11})} \right) \right], \qquad \text{(A5)}$$

$$X_2 = \left[- \frac{|\Gamma_G S_{21} S_{12}|^2}{|1 - \Gamma_G S_{11}|^2} + 1 - |S_{22}|^2 - 2\tan\zeta_2 \, Im S_{22} \right.$$

$$\left. - 2\,Re\left(\frac{S_{21} S_{12} \Gamma_G}{1 - \Gamma_G S_{11}} \, (S_{22}^* - j\tan\zeta_2) \right) \right]. \qquad \text{(A6)}$$

With a little effort and patience, these can be put in the form

$$X_1 = - \frac{|S_{21}|^2}{|1 - \Gamma_G S_{11}|^2} [1 - |\Gamma_G|^2 - 2 \tan\zeta_1 \, Im\Gamma_G] \, , \tag{A7}$$

$$X_2 = [1 - |\Gamma_{GS}|^2 - 2 \tan\zeta_2 \, Im\Gamma_{GS}] \, , \tag{A8}$$

with Γ_{GS} still given by eq (17). Referring back to eq (A1), we can use eqs (A2) and (A4) to write

$$P_2^{avail} = \alpha_{21} P_1^{avail} + \frac{[X_2 \cos^2\zeta_2 + X_1 \cos^2\zeta_1]}{[1 - |\Gamma_{GS}|^2 - 2 \, Im\Gamma_{GS} \tan\zeta_2] \cos^2\zeta_2} P_A \, . \tag{A9}$$

Substituting eqs (A7) and (A8) into eq (A9) then leads to the desired result,

$$P_2^{avail} = \alpha_{21} P_1^{avail} + [1 - \alpha_{21}] \, k_B B T_A \, . \tag{A10}$$

The derivation of eq (A10) or (25) is interesting for several reasons. For one thing, it constitutes a nice check that we know what we are doing and that the expressions we have derived for attenuation, wave amplitudes, etc. are at least consistent. It also provides an explicit, rather general, proof of eq (A10) and eq (25), without any assumptions about impedance matching, $S_{12} = S_{21}$, etc. Finally, it verifies that the correlation term $\langle \hat{b}_1 \hat{b}_2^* \rangle$ is properly included in the expression for P_2^{avail} in terms of α, eq (A10).

APPENDIX B

B.1 Some Pseudo-Wave Algebra

Before tackling the pseudo-wave noise equations, it is useful to review some of the basic algebra of pseudo-waves [15]. As a matter of notation, primes will be used to indicate pseudo-wave quantities in this appendix. The pseudo-wave amplitudes, a' and b', are obtained from the travelling-wave amplitudes, a and b, by the transformation

$$\begin{pmatrix} a' \\ b' \end{pmatrix} = Q \begin{pmatrix} a \\ b \end{pmatrix} , \tag{B1}$$

with

$$Q = \frac{1}{2}\left|\frac{Z_0}{Z'}\right|\sqrt{\frac{Re\,Z'}{Re\,Z_0}}\begin{pmatrix} 1+\frac{Z'}{Z_0} & 1-\frac{Z'}{Z_0} \\ 1-\frac{Z'}{Z_0} & 1+\frac{Z'}{Z_0} \end{pmatrix}, \qquad \text{(B2)}$$

and where Z_0 is the modal impedance of the travelling waves and Z' is the pseudo-wave reference impedance. Travelling waves at a given reference plane are labelled by a or b according to their direction of motion, or whether they are input or output. Pseudo-waves do not have a single direction of propagation, and so when we need some way of referring to the two components of the vector in eq (B1) we shall refer to them as either type-1 or type-2 pseudo-wave amplitudes (or pseudo-waves), according to whether they transform like the top or bottom component of the vector.

The pseudo-wave reflection coefficient is defined by

$$\Gamma' \equiv \frac{b'}{a'}. \qquad \text{(B3)}$$

We can derive the relationship between Γ' and the travelling-wave reflection coefficient Γ by using $b = \Gamma a$ in eq (B1), and then forming Γ' from eq (B3). The result is

$$\Gamma' = \frac{\gamma + \Gamma}{1 + \gamma\Gamma}, \qquad \text{(B4)}$$

with $\gamma = (Z_0-Z')/(Z_0+Z')$. The travelling-wave relation $a = \Gamma_G b + \hat{b}_G$ generates a corresponding pseudo-wave equation,

$$a' = \Gamma'_G b' + \hat{b}'_G, \qquad \text{(B5)}$$

where $\hat{b}'_G = N(1+Z'/Z_0)\hat{b}_G$ and Γ_G' is related to Γ_G by eq (B4). This can be seen by substituting $a = \Gamma_G b + \hat{b}_G$ in eq (B1) and solving for a'. Combining eqs (B3) and (B5) yields the expression for a' in terms of $\hat{b}'_G$,

$$a' = \frac{\hat{b}_G'}{1 - \Gamma_G'\Gamma_L'} , \tag{B6}$$

where Γ_L' is the pseudo-wave reflection coefficient of whatever is to the right of the reference plane.

Type-1 and type-2 pseudo-waves of a two-port between reference planes 1 and 2 are related by the pseudo-wave scattering matrix,

$$\begin{pmatrix} b_1' \\ b_2' \end{pmatrix} = S' \begin{pmatrix} a_1' \\ a_2' \end{pmatrix} + \begin{pmatrix} \hat{b}_1' \\ \hat{b}_2' \end{pmatrix} , \tag{B7}$$

where $\hat{b}_1'$, $\hat{b}_2'$ are the generator pseudo-wave amplitudes of the two-port. The pseudo-wave S-parameters and the generator pseudo-waves can be related to the travelling-wave S-parameters, but we will not need to use those relationships.

B.2 Power and Noise Equations

We can now work on the power and noise equations for pseudo-waves. The problem is as follows. Given that the travelling-wave equations derived in the text for measuring noise on wafer are valid, show that those same equations hold for pseudo-waves, provided that the pseudo-wave reflection coefficients and S-parameters are used and that the phase of the reference impedance is used in place of ζ. This amounts to proving the invariance of the on-wafer noise-temperature equations under pseudo-wave transformations. The equations of interest are virtually all the equations in subsections 2.2 through 2.4. Of these, the key equations are those for delivered power and available power, since equations for mismatch factors, available power ratios, and the radiometer equation all follow from the power expressions.

As in the travelling-wave case, we consider only reference planes at which only a single mode (in each "direction") is present. The pseudo-wave equation for delivered power at some reference plane [15] is given by

$$P^{del} = |a'|^2 [1 - |\Gamma'|^2 - 2\, Im\Gamma' \tan\zeta'] , \tag{B8}$$

where ζ' is the phase of Z'. This is the same form as the first part of eq (11) for the delivered power in terms of travelling-waves. To obtain the pseudo-wave version of the second part of eq (11), we simply use eq (B6) in eq (B8), which yields

$$p^{del} = \frac{|\mathcal{E}_G'|^2}{|1 - \Gamma' \Gamma_G'|^2} [1 - |\Gamma'|^2 - 2 \tan\zeta' \, Im\Gamma'] . \qquad \text{(B9)}$$

Thus eq (11) for delivered power is the general form for pseudo-waves, provided that pseudo-wave amplitudes, reflection coefficients, and reference impedance are used.

The expression for the available power is obtained from eq (B9) by using the (allowable) value of Γ' which maximizes p^{del},

$$p^{avail} = \frac{|\mathcal{E}_G'|^2}{|1 - \Gamma_{opt}' \Gamma_G'|^2} \left[1 - |\Gamma_{opt}'|^2 - 2 \tan\zeta' \, Im\Gamma_{opt}'\right] . \qquad \text{(B10)}$$

This is the same form as the equation for travelling waves, but that fact is not really significant since we have not yet given an expression for Γ_{opt}'. To prove that the expression for available power is invariant under pseudo-wave transformations we must show that the expression for Γ_{opt} is invariant. This is done by taking the travelling-wave equation for Γ_{opt},

$$\Gamma_{opt} = \frac{\Gamma_G^* - j \tan\zeta}{1 - j \Gamma_G^* \tan\zeta} , \qquad \text{(B11)}$$

and transforming it according to eq (B4) to obtain Γ_{opt}',

$$\Gamma_{opt}' = \frac{\gamma + \Gamma_{opt}}{1 + \gamma \Gamma_{opt}} . \qquad \text{(B12)}$$

With some tedious algebra (too boring even for an appendix), we can then show that

$$\Gamma_{opt}' = \frac{\Gamma_G'^* - j \tan\zeta'}{1 - j \Gamma_G'^* \tan\zeta'} . \qquad \text{(B13)}$$

This is the same form as eq (B11) or eq (12), and thus the equation for Γ_{opt} is invariant. As in the travelling-wave case, we can then use eq (B13) in eq (B10) to get

$$P^{avail} = \frac{|\hat{b}'_G|^2}{\left[1 - |\Gamma'_G|^2 - 2\,Im\Gamma'_G \tan\zeta'\right]\cos^2\zeta'}, \qquad \text{(B14)}$$

which is the same form as eq (13) for travelling waves. Thus the equations for both delivered and available power, derived for travelling waves, are valid for pseudo-waves as well.

The equations for delivered and available power, plus the algebraic relations of section 7.1 above, are all that is needed to derive the pseudo-wave versions of eqs (14) through (32) of the main text. The same steps are followed as for the travelling-wave development, and since the underlying equations all have the same form, so do the derived equations. As an example, if we set the available power, eq (B14), equal to $k_B BT$, we obtain the equation for the generator wave amplitude,

$$\langle|\hat{b}'_G|^2\rangle = k_B B T\left[1 - |\Gamma'_G|^2 - 2\,Im\Gamma'_G \tan\zeta'\right]\cos^2\zeta', \qquad \text{(B16)}$$

which is the same form as the travelling-wave equation, eq (14). All other equations are obtained by following the same steps as the travelling-wave development.

Therefore, the power and noise equations derived for travelling waves in the main text are valid for pseudo-waves as well, provided that the pseudo-wave reflection coefficients and S-parameters are used and that the pseudo-wave reference impedance is used in place of the characteristic impedance of the mode.

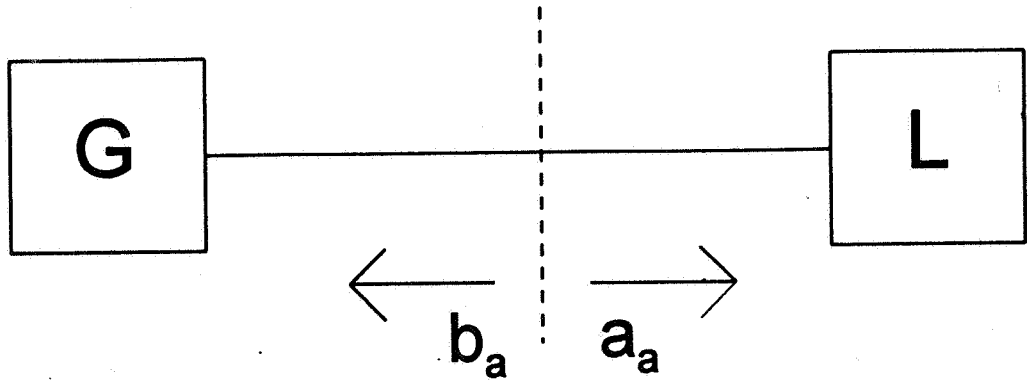

Figure 1. Lossy line connecting generator and load. Subscripts refer to mode.

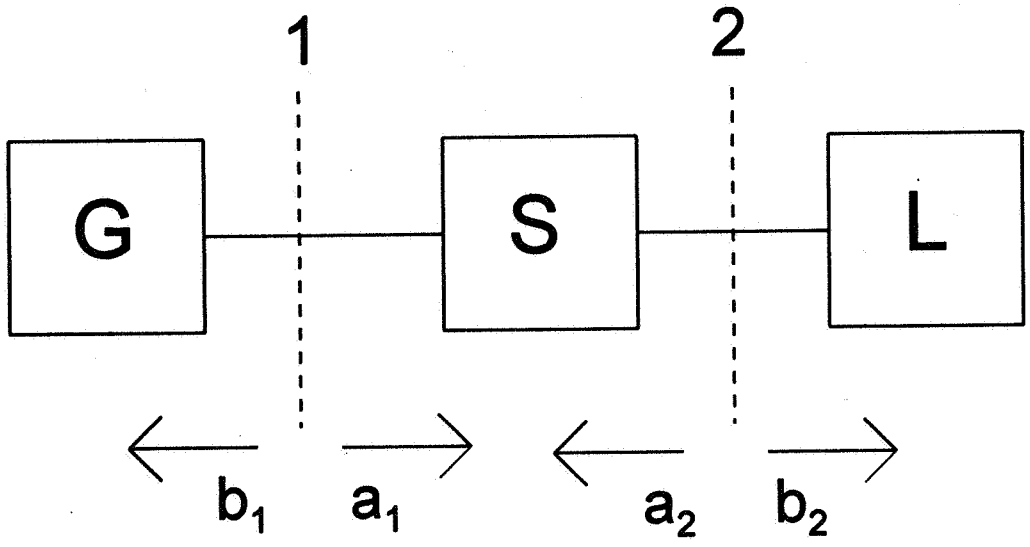

Figure 2. Two-port between generator and load. Subscripts refer to reference plane.

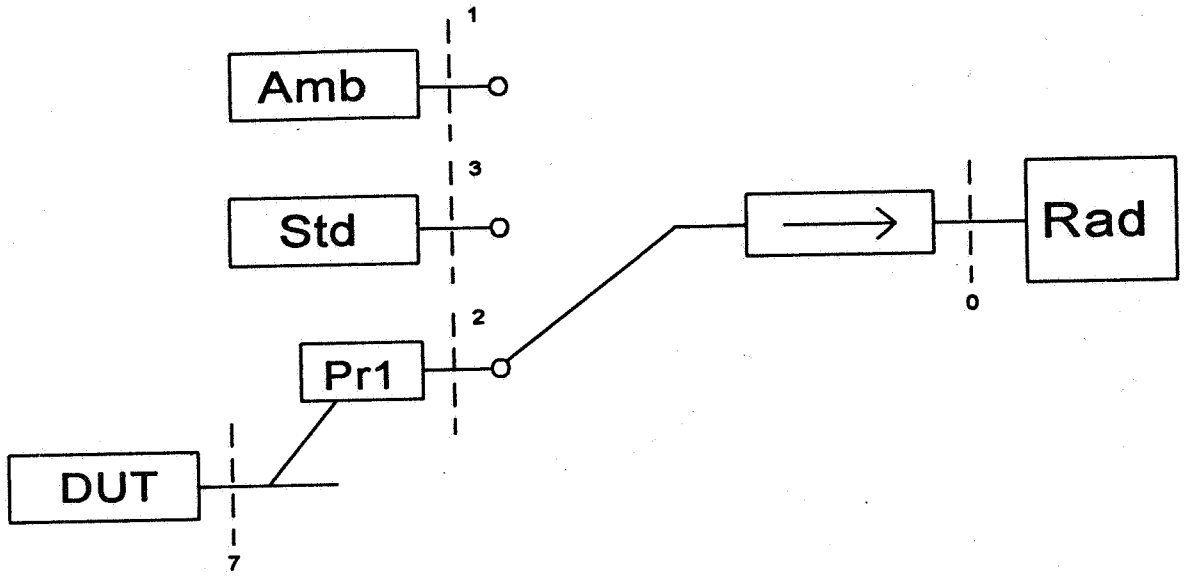

Figure 3. Basic setup for measurement of on-wafer noise source.

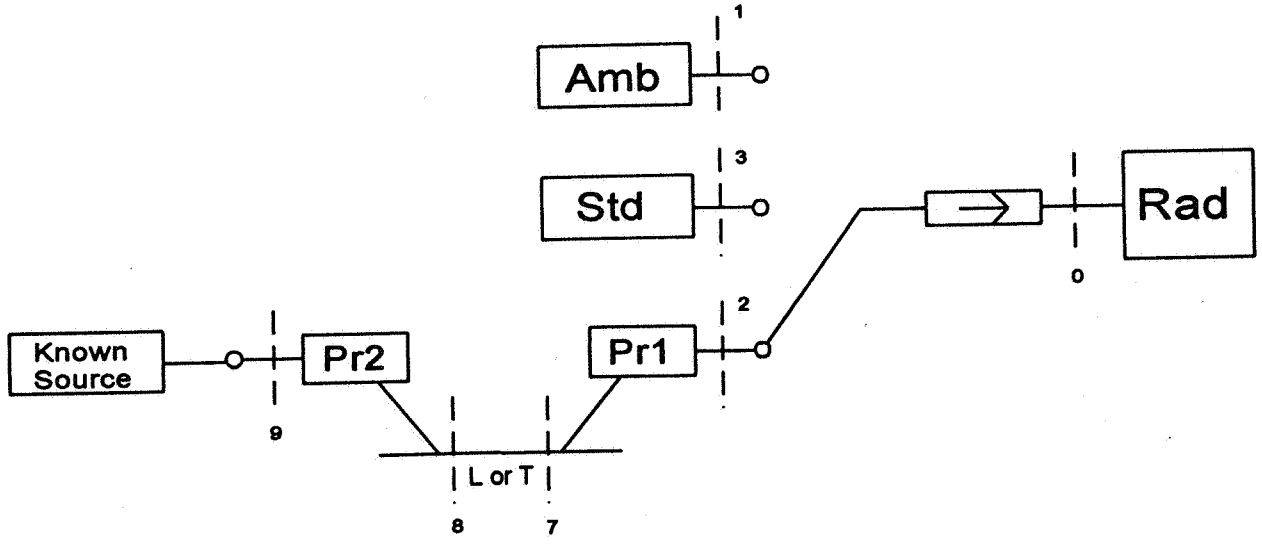

Figure 4. Basic setup for measurements of known on-wafer noise temperatures from off-wafer standards.

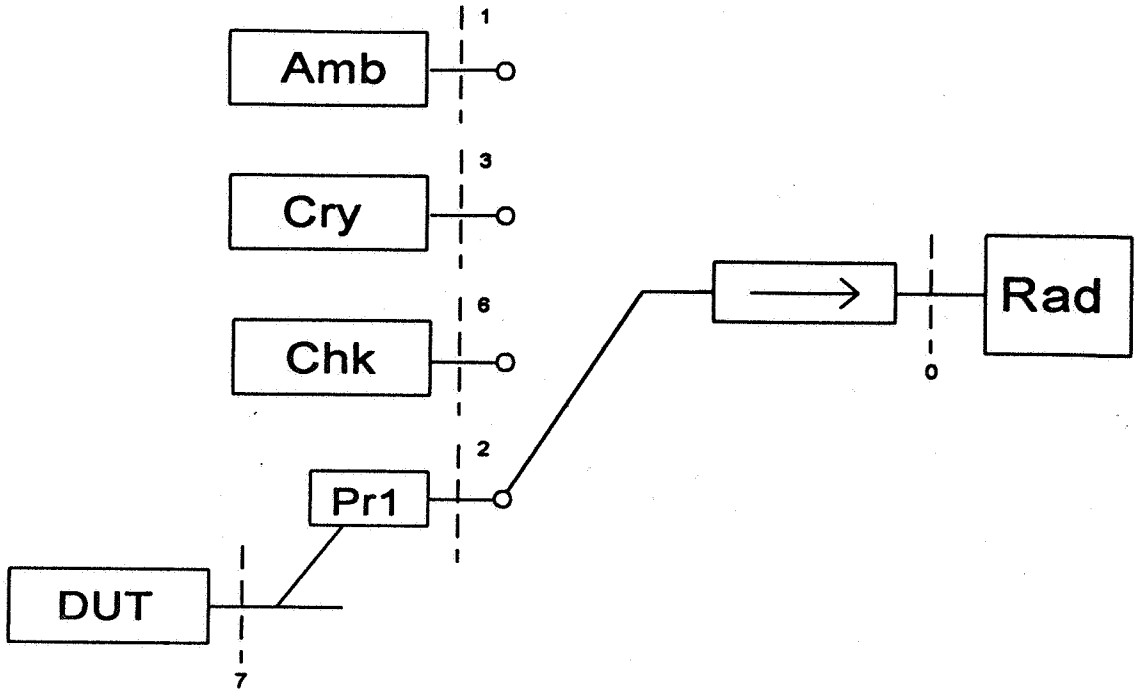

Figure 5. Configuration for measurement of on-wafer noise temperature.

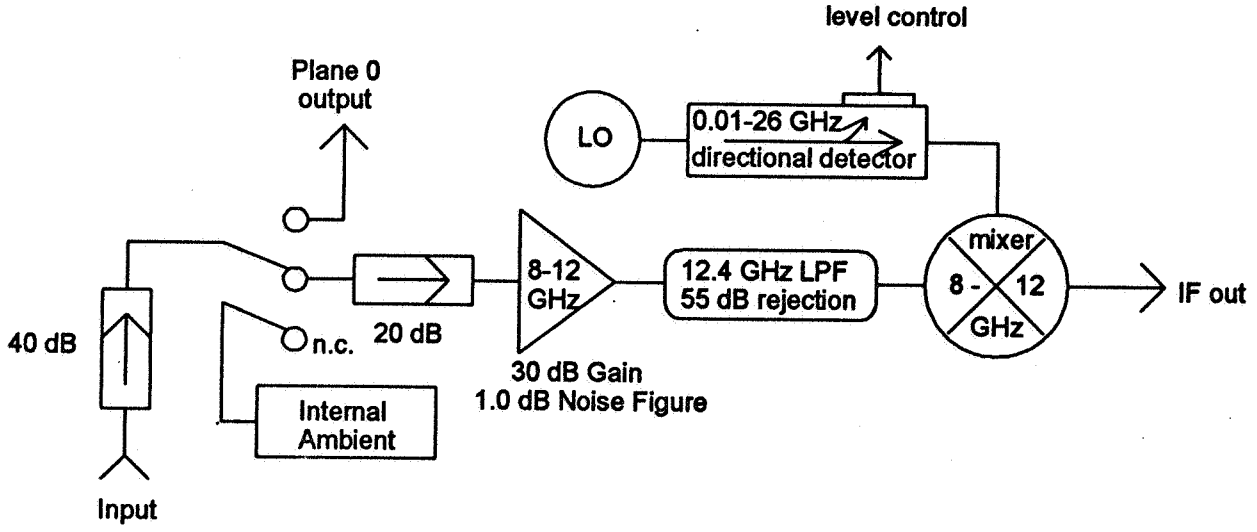

Figure 6. Detail of radiometer.

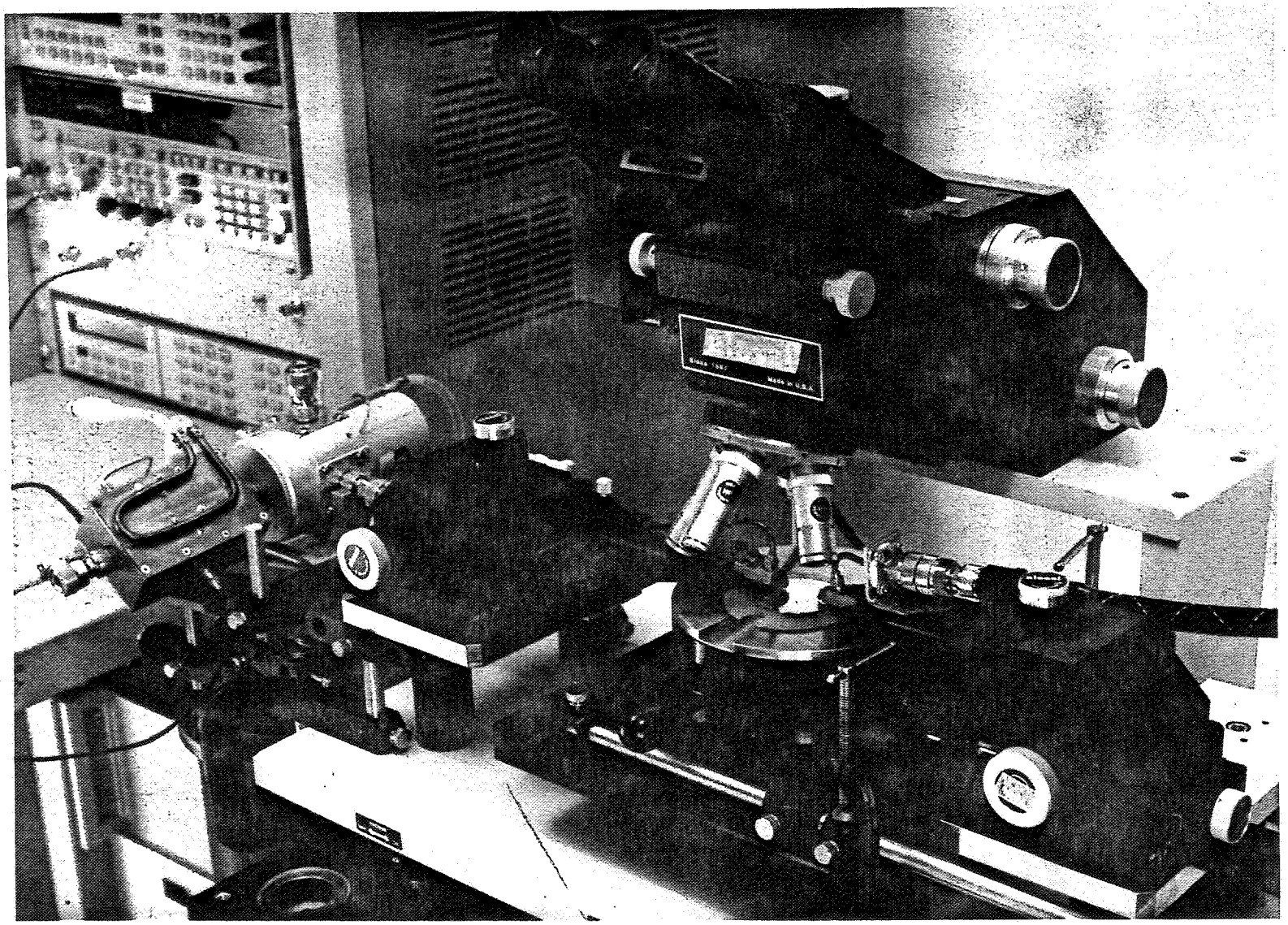

Figure 7. Closeup of measurement setup.

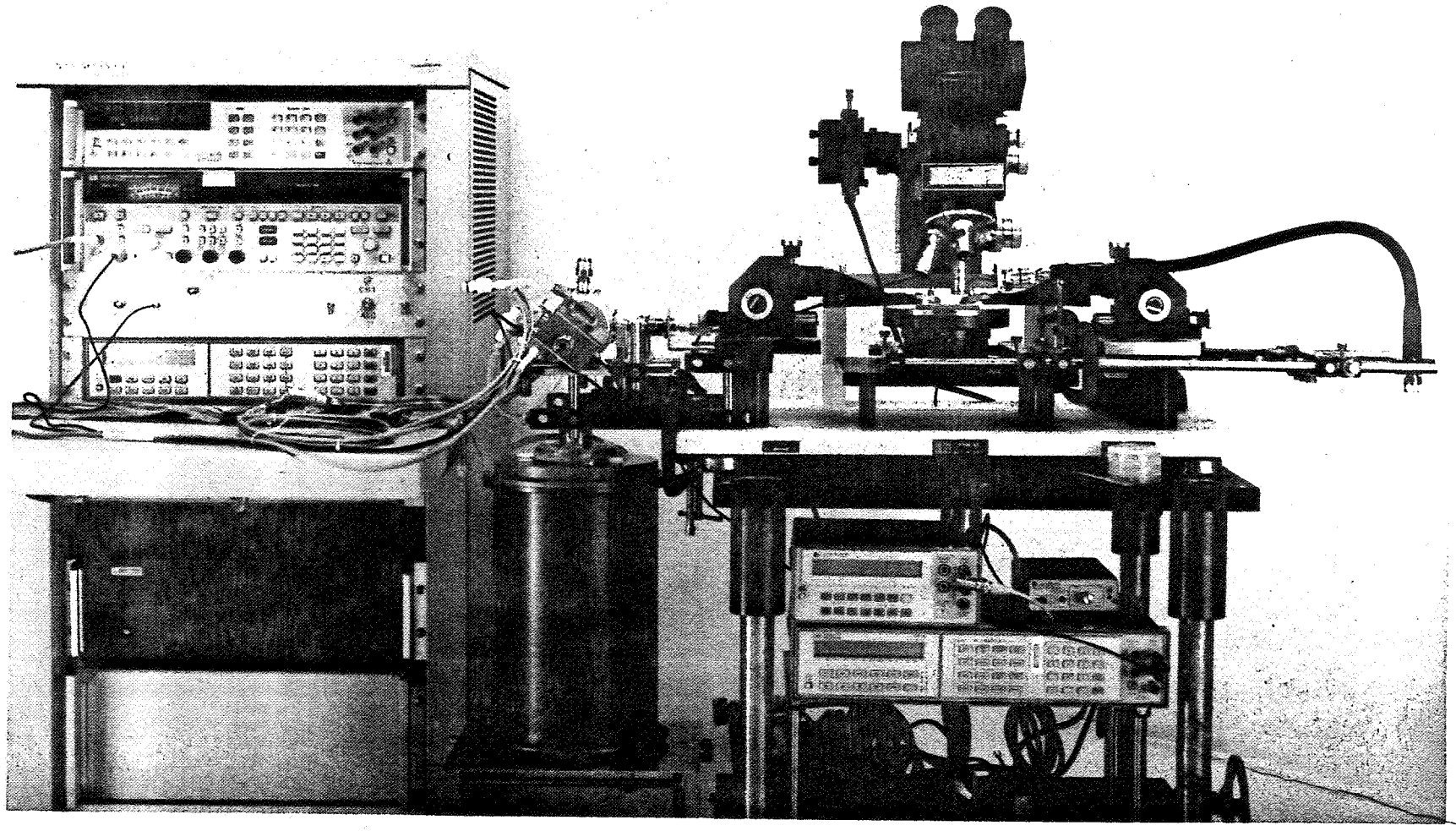

Figure 8. Full view of measurement setup.

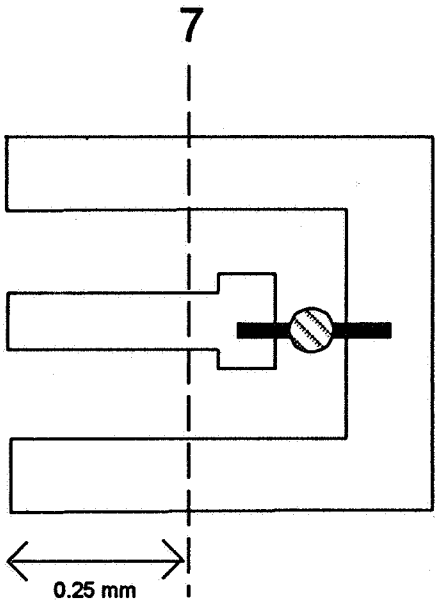

Figure 9. On-wafer noise diode (shaded circle) bonded to coplanar waveguide.

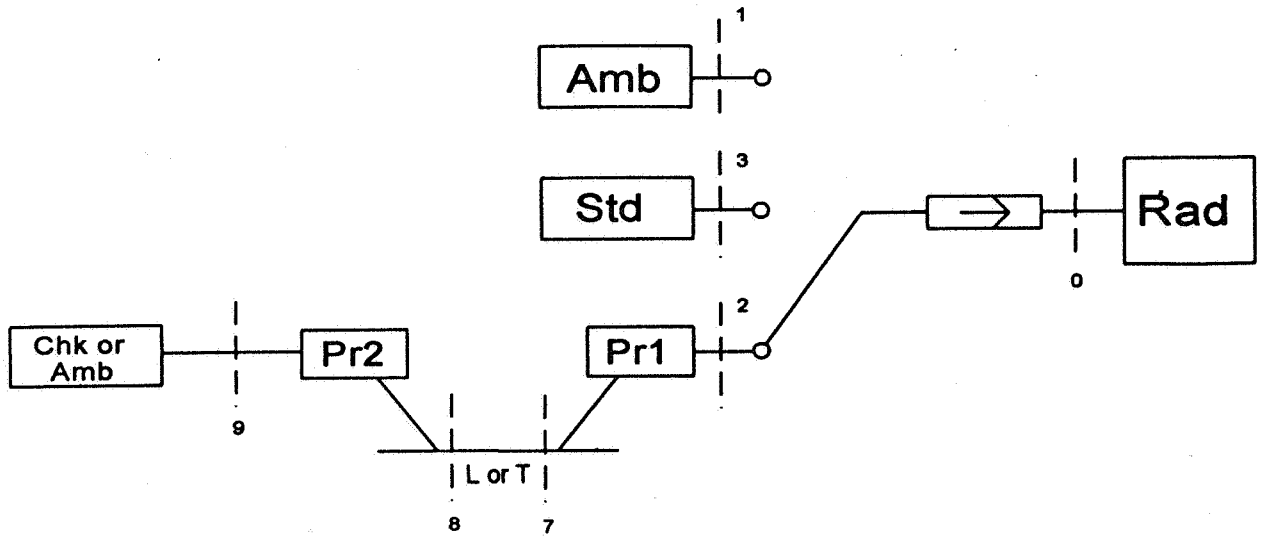

Figure 10(a). Configuration for producing known noise temperature on wafer.

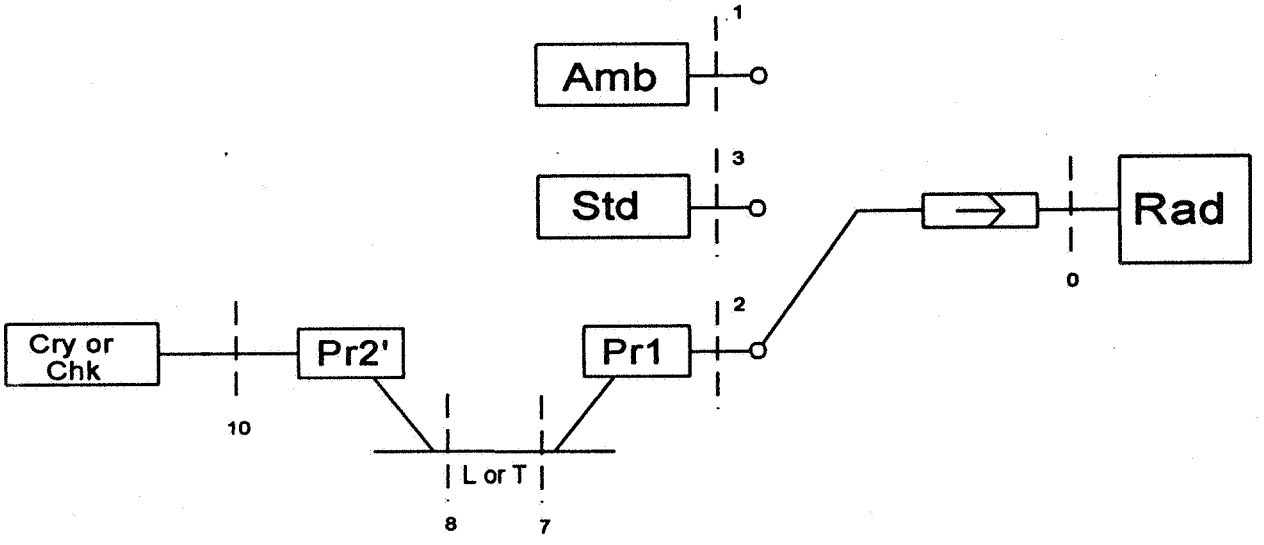

Figure 10(b). Alternate configuration for producing known noise temperature on wafer. Pr2' consists of Pr2 plus a length of flexible cable.

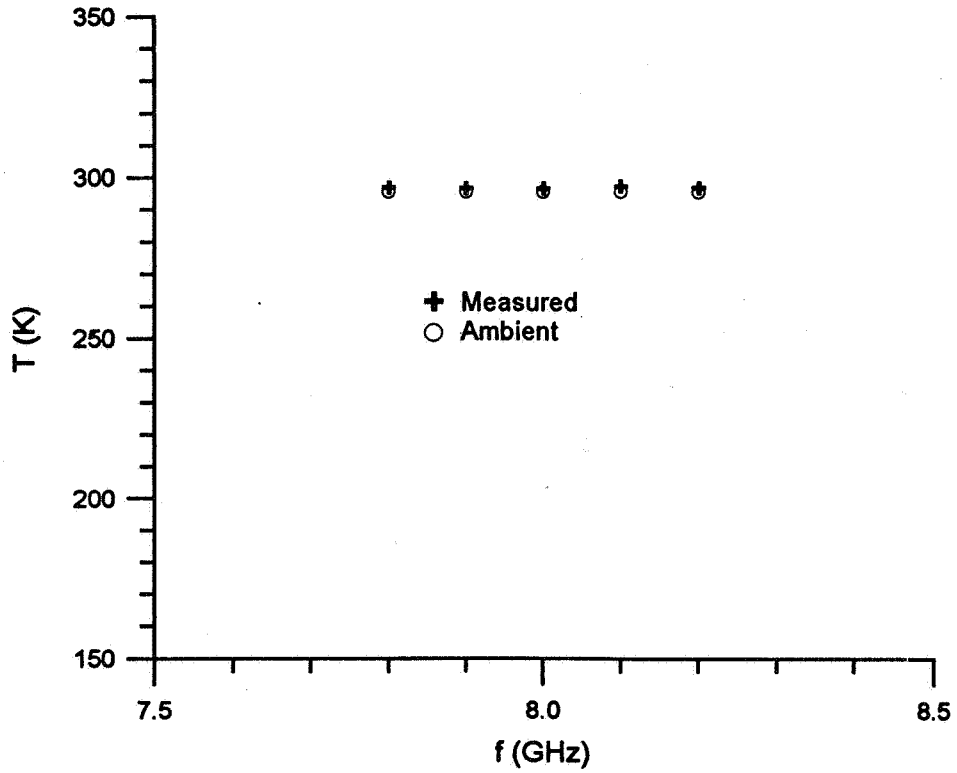

Figure 11(a). On-wafer noise temperature for configuration using on-wafer room-temperature resistor (7R).

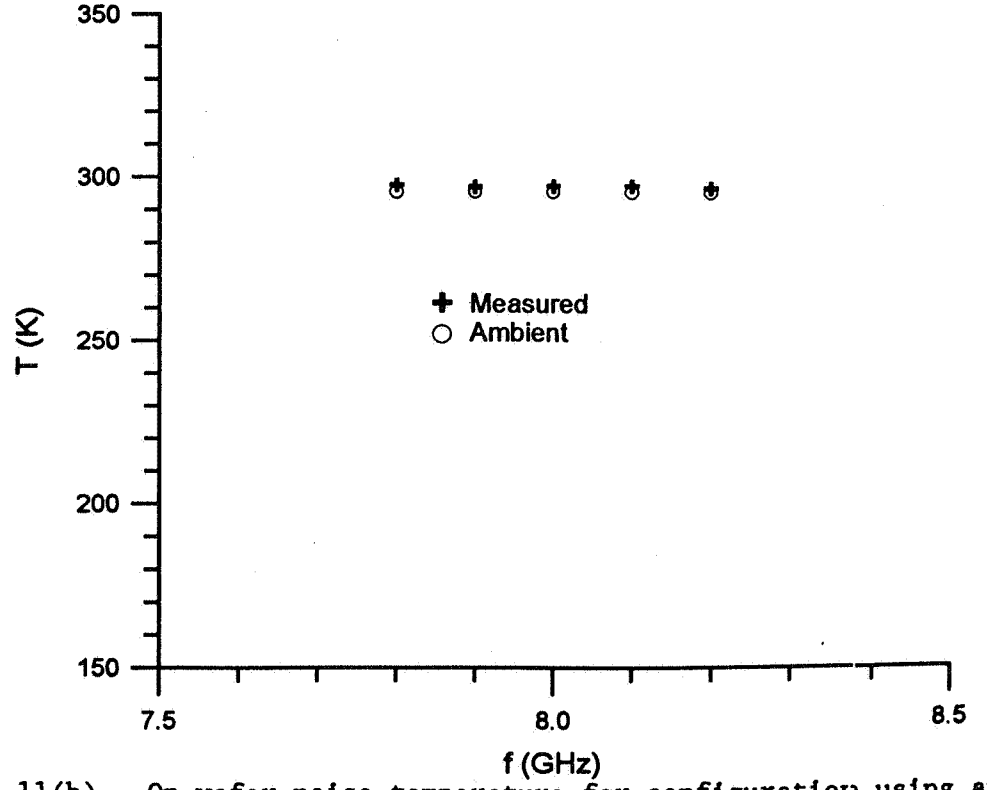

Figure 11(b). On-wafer noise temperature for configuration using ambient source, on-wafer through (7T9A).

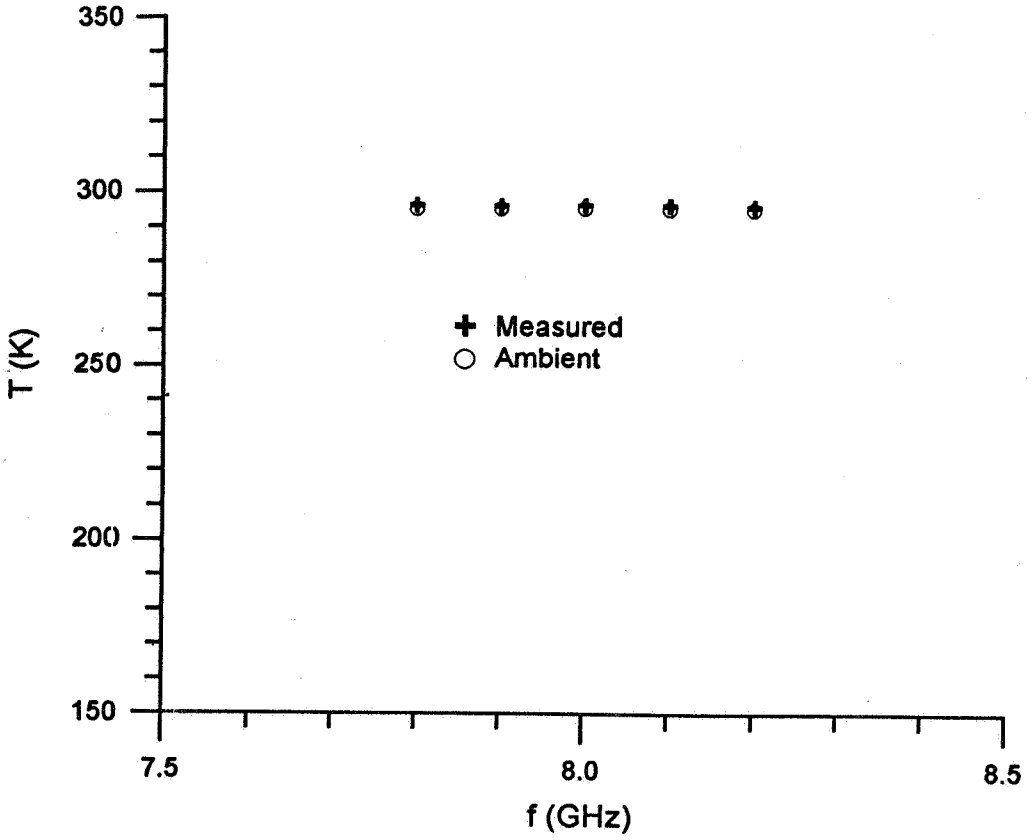

Figure 11(c). On-wafer noise temperature for configuration using ambient source, line on wafer (7L9A).

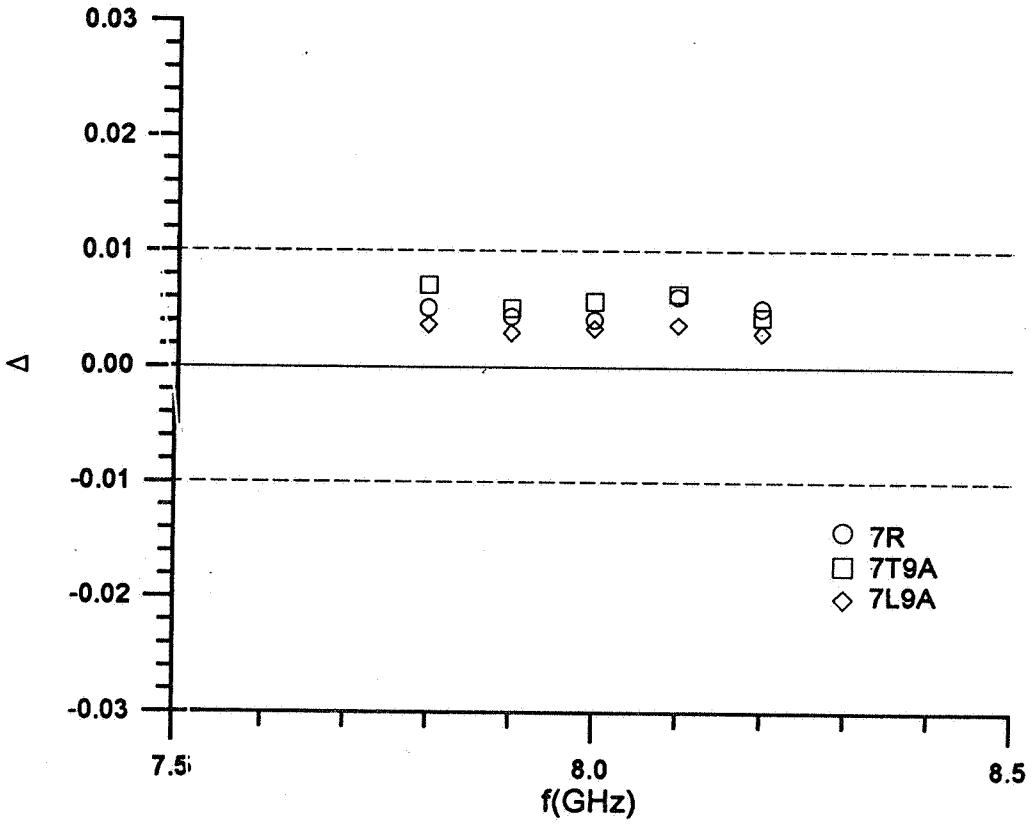

Figure 12. Fractional differences between measured and predicted on-wafer noise temperatures for ambient sources.

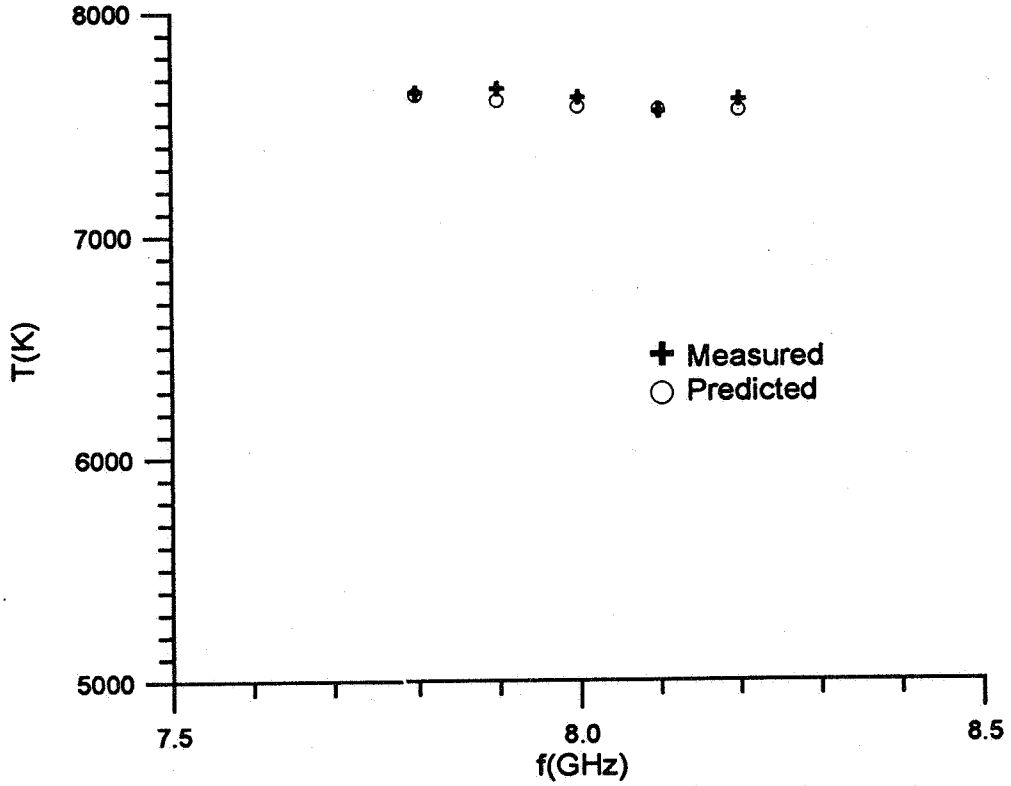

Figure 13(a). On-wafer noise temperature for configuration using high-temperature source, on-wafer through (7T9Ck).

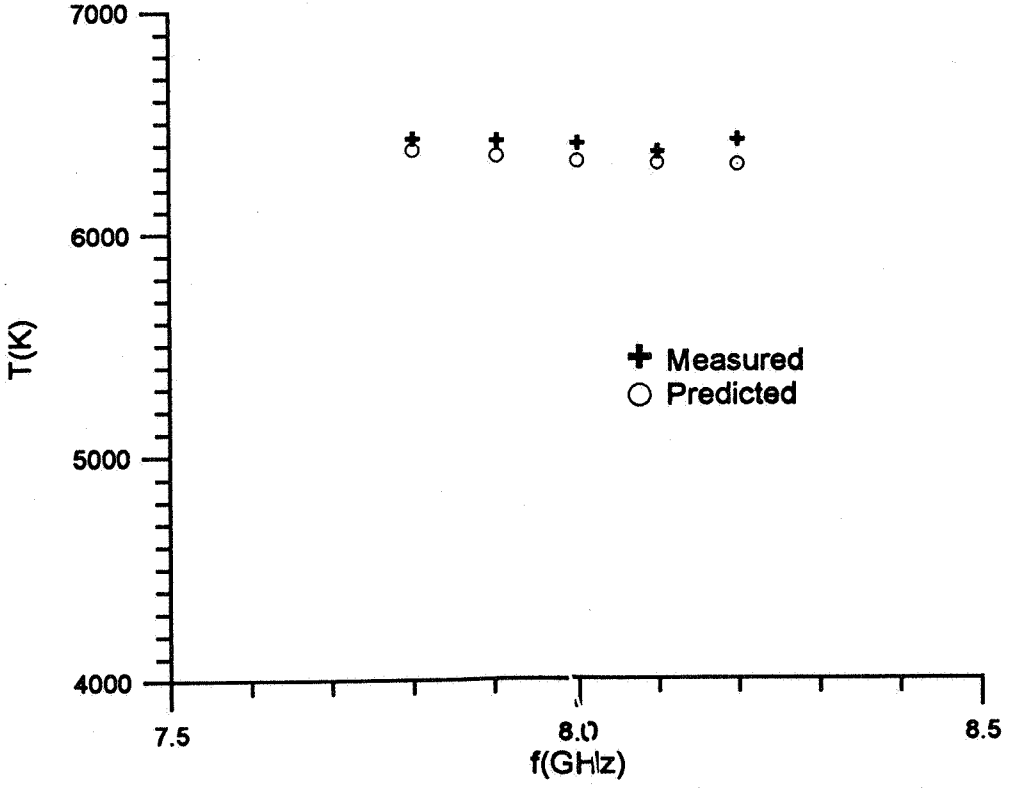

Figure 13(b). On-wafer noise temperature for configuration using high-temperature source, on-wafer line (7L9Ck).

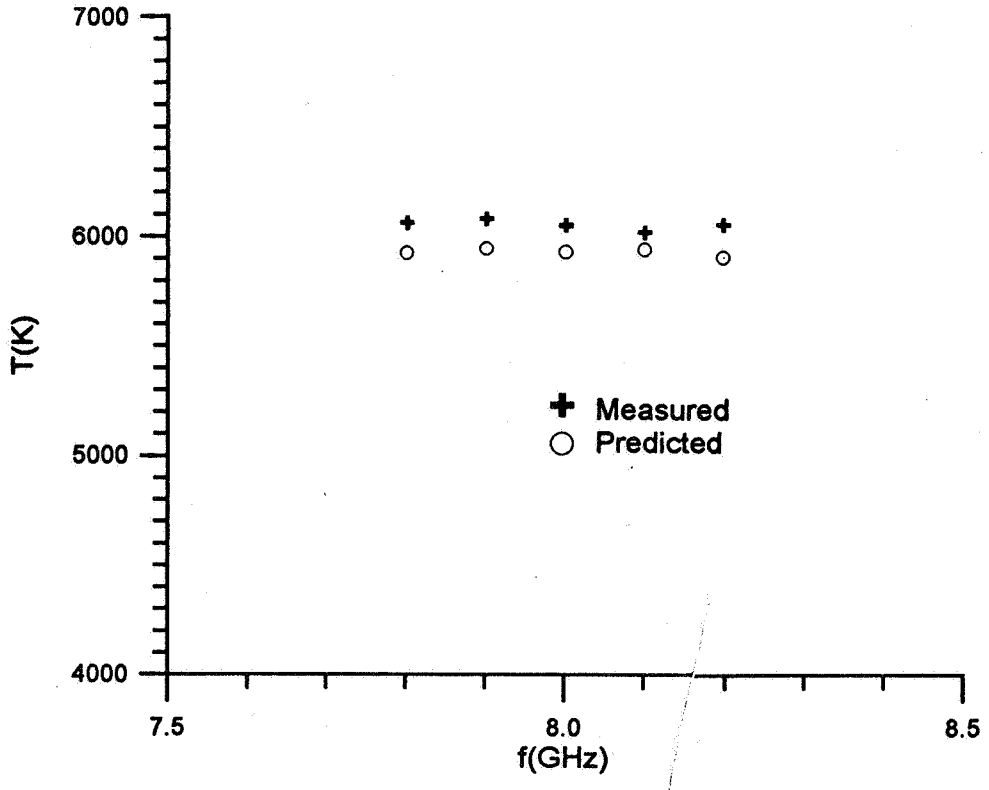

Figure 14(a). On-wafer noise temperature for configuration using high-temperature source, cable, on-wafer through (7T10Ck).

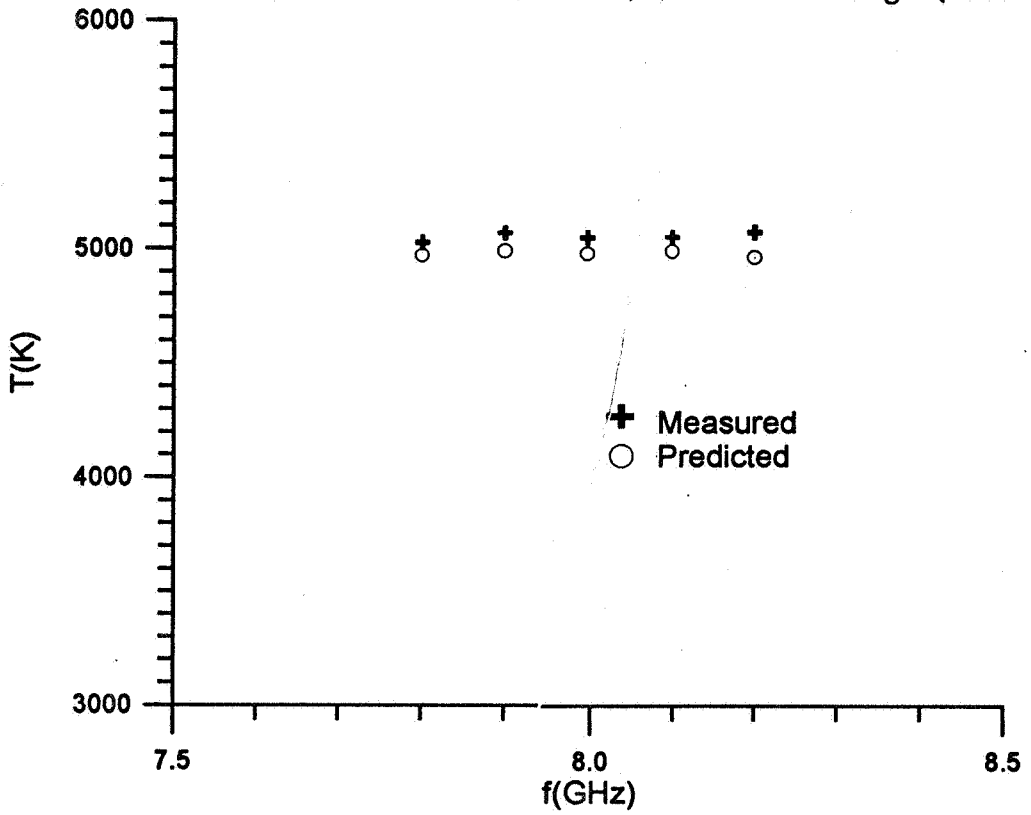

Figure 14(b). On-wafer noise temperature for configuration using high-temperature source, cable, on-wafer line (7L10Ck).

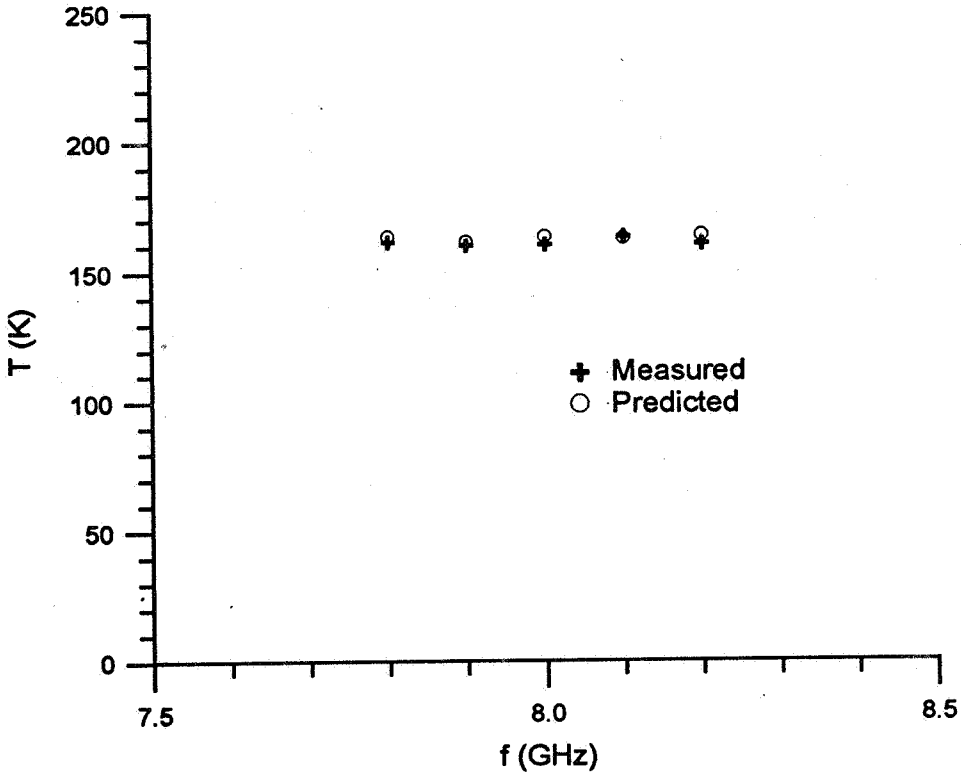

Figure 15(a). On-wafer noise temperature for configuration using cryogenic source, cable, on-wafer through (7T10Cr).

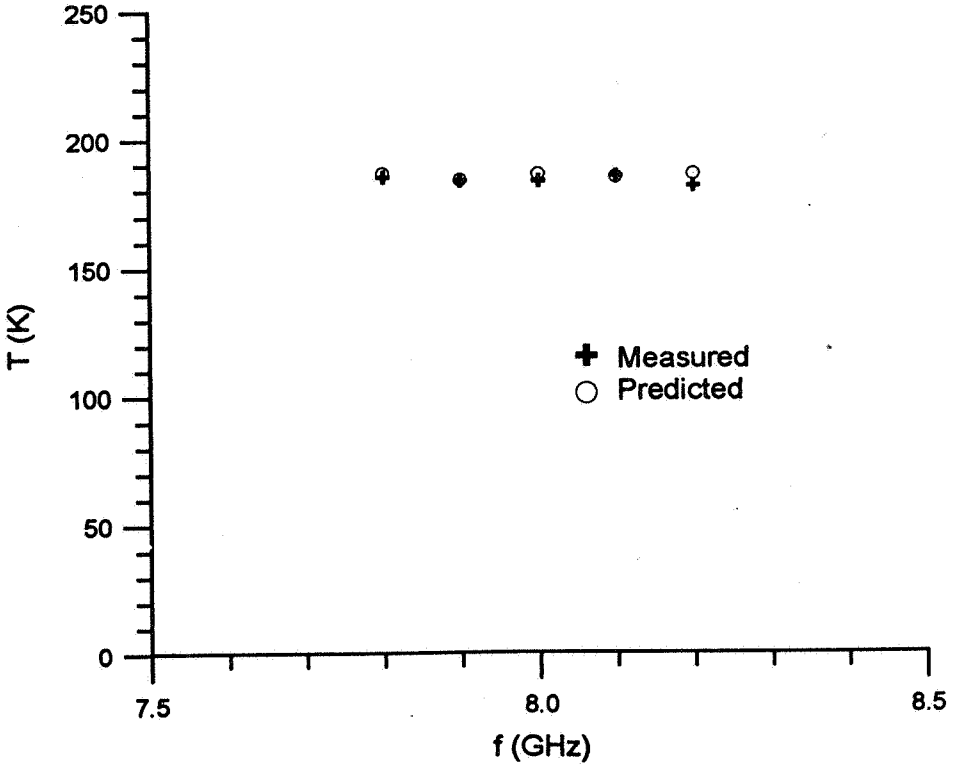

Figure 15(b). On-wafer noise temperature for configuration using cryogenic source, cable, line on wafer (7L10Cr).

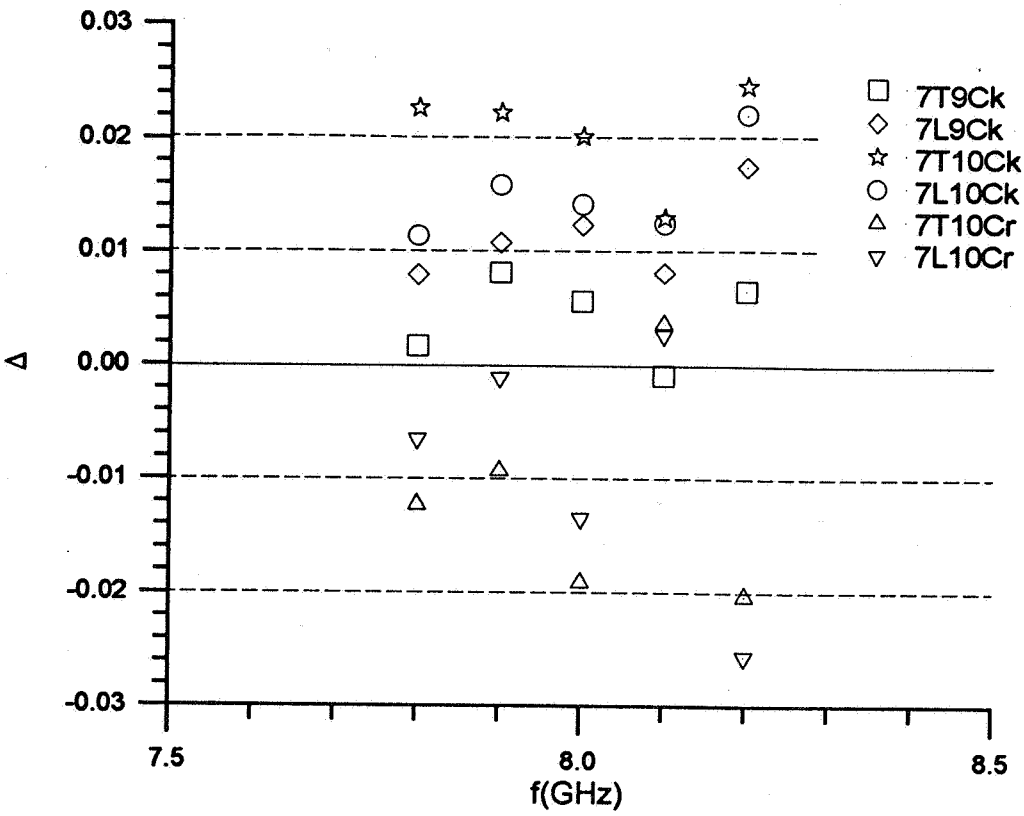

Figure 16. Fractional differences between measured and predicted on-wafer noise temperatures for nonambient sources.

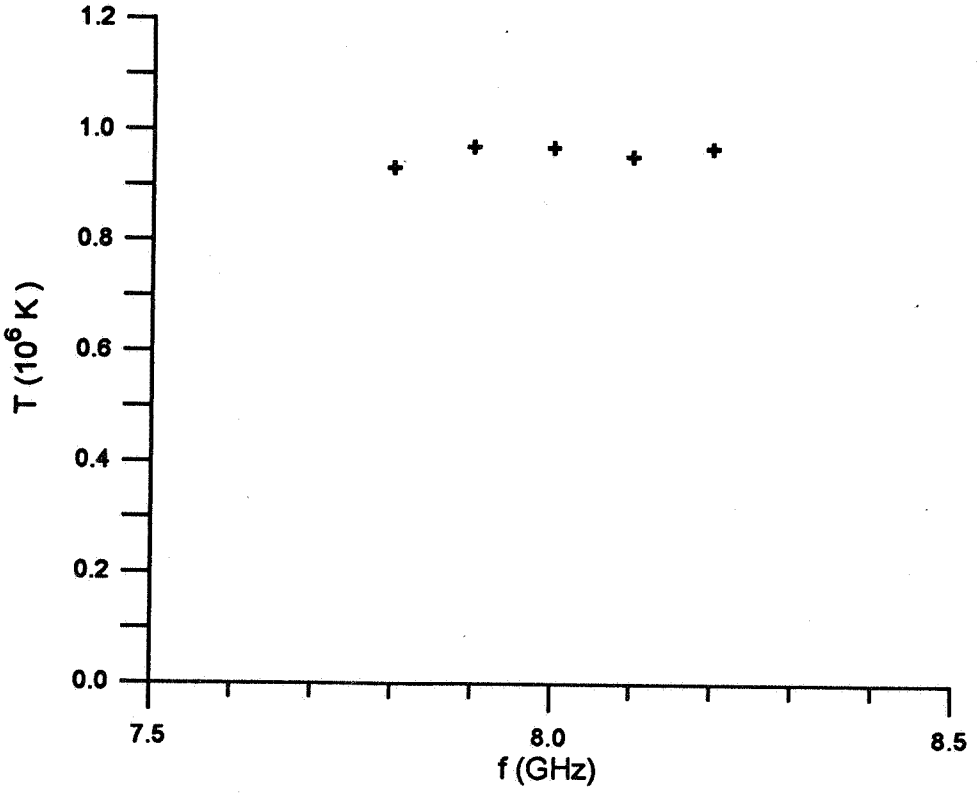

Figure 17. Measured noise temperature of on-wafer noise diode (7D).

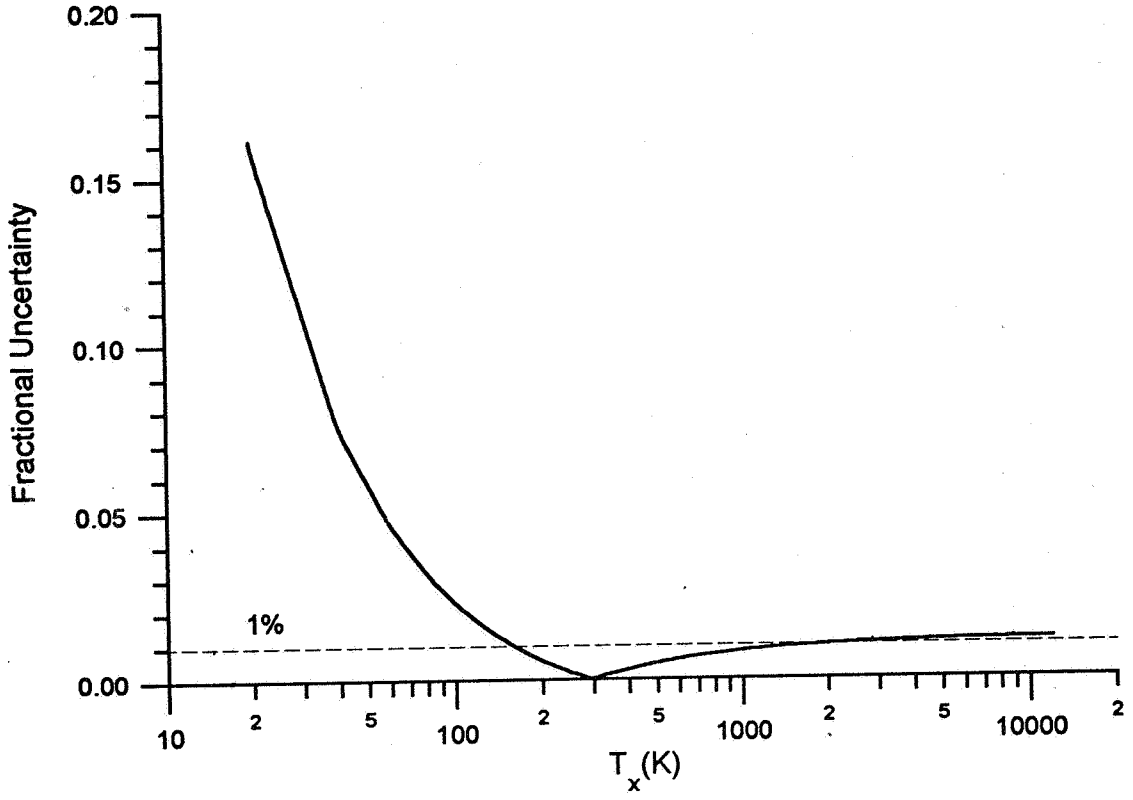

Figure 18(a). Fractional uncertainty (1σ) in on-wafer noise-temperature measurements.

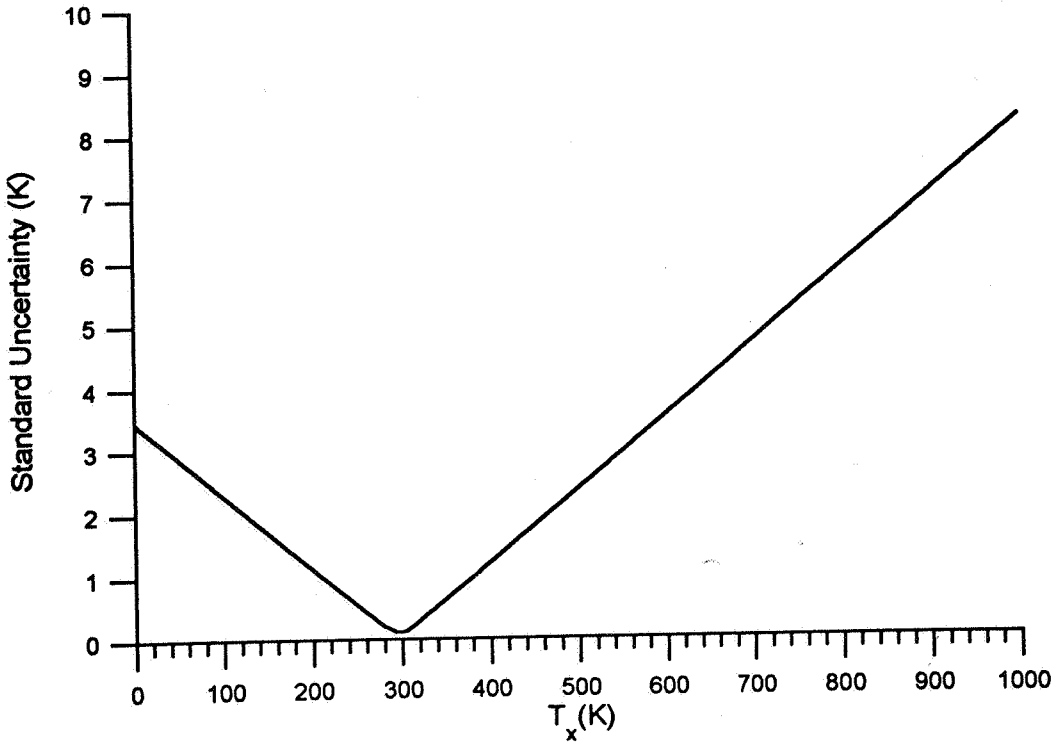

Figure 18(b). Absolute uncertainty (1σ) in on-wafer noise-temperature measurements.

*U.S. GOVERNMENT PRINTING OFFICE:575-245/65045